



**KTH Architecture and
the Built Environment**

Numerical analysis of laterally loaded lime/cement columns

Benjamin Charbit

Master of Science Thesis 09/05
Division of Soil and Rock Mechanics
Department of Civil and Architectural Engineering

Stockholm, Sweden, 2009

© Benjamin Charbit 2009
Master of Science Thesis 09/05
Division of Soil and Rock Mechanics
Royal Institute of Technology (KTH)
ISSN 1652-599X

i would not want
t' be bach. mozart. tolstoy. joe hill. gertrude
stein or james dean/they are all dead. the
Great books' ve been written. the Great sayings
have all been said

Bob Dylan

Abstract

Stabilization of soft clayey soils with lime/cement columns has become a common ground improvement method in Europe, USA and Japan. Yet, the current design methods considering stability analyses show limitations, in that they only consider shear failure of the columns. Previous experimental and theoretical studies have showed that failure by bending is more probable. In this thesis shearing tests on reinforced clay are reproduced with non-linear finite element modeling. The new material model used for lime/cement makes it possible to simulate and observe cracks within the columns. Numerical analyses on unreinforced soil are first performed as a mean of calibrating material parameters, and then lime/cement column stabilized soils are simulated.

The results obtained showed good agreement with the reduced-scale laboratory model tests. They confirm the general conclusions regarding failure of the columns, and can be used as a link towards a more realistic design method.

Keywords: deep mixing soil stabilization, finite element method, lime/cement, clay, damaged plasticity, reduced-scale test

Sammanfattning

Djupstabilisering av leriga jordar med kalkcementpelare är idag en vanlig jordförstärkningsmetod i bland annat Skandinavien, USA och Japan. De dimensioneringsmetoder som används i Sverige för brottstadianalyser är dock bristfälliga eftersom de endast beaktar skjuvbrott i pelarna. Flera experimentella och teoretiska studier har dock visat att det är mer sannolikt med böjbrott vilket kan medföra att man kan ha underdimensionerat konstruktioner. I detta examensarbete har tidigare utförda skjuvboxförsök på kaolinlera förstärkt med kalk/cement simulerats med icke-linjär finit elementmetod. En ny materialmodell som möjliggör simulering och observation av sprickor i pelarna har använts för kalkcementpelarna. Numeriska analyser på oförstärkt kaolinlera utfördes först för att kalibrera materialparametrarna och därefter simulerades kaolinlera förstärkt med kalkcementpelare. Resultaten från simuleringarna visar en god överensstämmelse med skjuvboxförsöken. De verifierar de generella antagandena avseende pelarnas brottmekanism och kan användas som underlag för att skapa en mer realistisk dimensioneringsmetod för jord förstärkt med kalk/cement.

Nyckelord: djupstabilisering, finita elementmetoden, kalkcementpelare, lerjord, damaged plasticity, skjuvboxförsök

Résumé

La stabilisation de sols argileux à l'aide de colonnes de chaux/ciment est une méthode répandue en Scandinavie et au Japon. Les réglementations en vigueur sont cependant imparfaites car elles supposent que la rupture des colonnes a lieu par cisaillement. Plusieurs études expérimentales et théoriques ont pourtant montré que la rupture par dépassement de la résistance à la flexion est plus probable. Dans cette thèse de mastère, plusieurs essais de cisaillement sont numériquement reproduits à l'aide de la méthode non linéaire des éléments finis. Le mélange de chaux/ciment est modélisé à l'aide d'un nouveau modèle permettant de simuler et d'observer les fissures qui se forment dans les colonnes. Des simulations sur des sols non renforcés sont dans un premier temps réalisées. Les sols stabilisés par des colonnes de chaux/ciment sont ensuite simulés.

Les résultats obtenus sont en accord avec les tests à échelle réduite réalisés en laboratoire. Ils confirment également les conclusions concernant les modes de rupture des colonnes, et peuvent servir de base pour le développement d'une réglementation plus réaliste.

Mots-clés: stabilisation des sols, méthode des éléments finis, chaux/ciment, argile, plasticité, dommages

Preface

The research work presented in this thesis was carried out from January 2009 to August 2009 at the Department of Civil and Architectural Engineering, Royal Institute of Technology (KTH). It ends my studies at KTH as well as at the École Centrale Marseille.

First of all, I express my gratitude to my supervisors, Stefan Larsson, for introducing me to this project and to the world of soil mechanics and geotechnics, and Anders Ansell. The guidance and help they provided during this thesis were very important to me.

I especially want to thank Richard Malm and Mahir Ülker Kaustell for helping me understanding and developing this project and for their valuable advice.

I also thank my international coordinator Åsa Carlsson and the Department of Civil and Architectural Engineering for welcoming me during the last two years and making my stay in Sweden so enjoyable.

I am also grateful to the Department of International Mobility at the École Centrale Marseille for making my exchange studies possible.

Last but not least I want to thank my family and friends wherever they are and especially my sisters and parents.

Stockholm, August 2009

Benjamin Charbit

Notations

Latin upper case letters

\mathbf{D}_0^{el}	initial elastic stiffness
\mathbf{D}^{el}	degraded elastic stiffness
E_{col}	modulus of elasticity of a columns (Pa)
E_0	initial modulus of elasticity (Pa)
F	yield function
G	plastic flow potential
G_f	fracture energy (N/m)
I_1	first invariant of stress tensor (Pa)
J_2	second invariant of stress deviator (Pa ²)
J_3	third invariant of stress deviator (Pa ³)
K_0	tangent stiffness
M_{clay}	odometer modulus of clay (Pa)
M_u	bending moment capacity of a column (Nm)
R_{mc}	Mohr-Coulomb deviatoric stress measure
R_{mw}	deviatoric elliptic function

Latin lower case letters

a	area ratio of the columns (m)
c	cohesion of the material (Pa)
$c_{u,\text{col}}$	undrained shear strength of lime/cement (Pa)
$c_{u,\text{clay}}$	undrained shear strength of clay (Pa)
d	column diameter (m)
d_t	damage variable in tension
d_c	damage variable in compression
d	stiffness degradation variable
f	distance between the failure surface and the plastic hinge (m)
k	bearing capacity factor
l_0	one unit length (m)
p	hydrostatic pressure stress, first coordinate in the (p, q, r) system (Pa)
q	Mises equivalent stress, second coordinate in the (p, q, r) system (Pa)
q_n	normal load over total area (Pa)
r	third coordinate in the (p, q, r) system (Pa)
\mathbf{s}	stress deviator
s_1, s_2, s_3	principal values of stress deviator (Pa)
u_{t0}	final cracking displacement (m)

u_t^{ck}	cracking displacement (m)
u_t^{pl}	plastic displacement (m)
w_t	tensile stiffness weight factor
w_c	compressive stiffness weight factor

Greek lower case letters

ε	flow potential eccentricity in meridional plane
$\tilde{\varepsilon}^{pl}$	equivalent plastic strain
ε_t	plastic strain in tension
$\tilde{\varepsilon}_t^{pl}$	equivalent plastic strain in tension
$\tilde{\varepsilon}_t^{ck}$	cracking strain
ε_c	plastic strain in compression
$\tilde{\varepsilon}_c^{pl}$	equivalent plastic strain in compression
ε_{0c}^{el}	elastic strain corresponding to undamaged material
$\tilde{\varepsilon}_c^{in}$	inelastic strain
θ	Lode angle
$d\lambda$	plasticity multiplier
ν	Poisson's ratio
ξ	first of the Haigh-Westergaard coordinates (Pa)
ρ	second of the Haigh-Westergaard coordinates (Pa)
σ	stress tensor
$\bar{\sigma}$	effective stress tensor
$\sigma_1, \sigma_2, \sigma_3$	principal values of stress tensor (Pa)
σ	normal stress on failure plane (Pa)
σ_t	uniaxial tensile stress (Pa)
$\bar{\sigma}_t$	effective tensile cohesion stress (Pa)
$\bar{\sigma}_t(\tilde{\varepsilon}_t^{pl})$	effective tensile cohesion stress
σ_{t0}	uniaxial tensile failure stress (Pa)
σ_c	uniaxial compressive stress (Pa)
$\bar{\sigma}_c$	effective compressive cohesion stress (Pa)
$\bar{\sigma}_c(\tilde{\varepsilon}_c^{pl})$	effective compressive cohesion stress (Pa)
σ_{c0}	initial uniaxial compressive yield stress (Pa)
σ_{b0}	initial equibiaxial compressive yield stress (Pa)
$\hat{\sigma}_{max}$	maximum principal effective stress (Pa)
τ	shear stress on failure plane (Pa)
φ	angle of internal friction (°)
ψ	dilation angle in meridional plane (°)

Others

$\langle \ \rangle$	Macauley bracket
C3D4	first-order tetrahedral elements
DMM	deep-mixing method
FE	finite element
U _i (i=1,2,3)	translation in the i-direction
UR _i	rotation about the i-direction

Contents

Abstract	i
Sammanfattning	iii
Résumé	v
Preface	vii
Notations	ix
1 Introduction	1
1.1 Background.....	1
1.2 Aim and scope of work	2
2 Laboratory tests	3
2.1 Procedure.....	3
2.2 Results	7
3 Review of previous work	9
3.1 Design methods	9
3.2 Limitations of the design methods	11
4 Finite Element analyses	15
4.1 The Finite Element Program ABAQUS	15
4.2 Material modeling in ABAQUS	16
4.2.1 Brief summary of continuum mechanics.....	16
4.2.2 Lime/cement improved kaolin	17
4.2.3 Clay.....	27
4.2.4 Sand	31
4.3 Numerical analyses.....	31
4.3.1 Non-linear analyses.....	31
4.3.2 Contact properties.....	32
4.3.3 Finite elements	35

4.3.4	Procedure	35
5	Results and discussion	39
5.1	Finite Element analyses of unstabilized soil.....	39
5.2	Finite Element analyses of stabilized soil.....	43
6	Conclusions	51
6.1	General conclusions.....	51
6.2	Suggestions for future research	52
	Bibliography.....	53

1 Introduction

1.1 Background

Deep stabilization of soft clay and organic soils using lime/cement columns has been an increasingly used ground improvement method since its introduction in the 1970's. Lime/cement columns is one of many methods, with the generic term “Deep mixing”, where binding agents, often lime or/and cement, are mechanically mixed with the soil (Porbaha, 1998; Terashi, 2003; Larsson, 2005). Lime/cement columns are frequently used in the construction of roads and railway embankments or lightweight structures on soft soil, especially in Scandinavia, Japan and the United States. Their main effects are to accelerate construction by eliminating the consolidation times, decrease settlements and improve embankment stability. It is often an economical solution compared with other soil improvements methods such as excavation and replacement and embankment piles. Lime/cement columns is the most common ground improvement method used in Sweden where soft sediments are common.

Lime/cement columns have progressively replaced lime columns since the 1990's and are nowadays almost systematically used. The existing code in Sweden is based on lime column properties, and on the assumption that the columns fully interact with the unstabilized soil between them, that is, the reinforced soil behaves as a composite material (SGF, 2000; Vägverket, 2009). Limit equilibrium slip circle analyses of slope stability are then performed using the composite strength of the improved ground. However, as discussed by Kivelö (1998), this method has shown practical limitations. One of the reasons is that the properties of lime columns are not identical to those of lime/cement columns. The shear strength and the modulus of elasticity are much higher and the failure strain is reduced when cement is added. Another reason is the assumption of full interaction between soil and columns, as pointed out by Kivelö (1998) and Broms (1999). Based on Broms (1972), Kivelö suggested that a lime/cement column behaves more like a pile when laterally loaded. He also presented several failure modes in the internal stability – shear, bending and tensile failure. For the external stability, centrifuge model studies and finite element (FE) analyses showed that the improved ground is more likely to fail with a collapse failure pattern than a sliding failure pattern (Kitazume and Maruyama, 2006). However, the current design methods (limit equilibrium analyses) only capture the effect of shear failure mode for the internal stability and of sliding failure for the external stability. Since those might not be the most probable failure causes, the current practice can substantially overestimate the stability of column-supported embankments. Numerical methods have been used to study the stability of embankments founded on deep-mixed columns by e.g. Kitazume and Maruyama (2006). Filz and Navin (2006) presented a good review of the existing works. The most commonly used software are the finite

difference program FLAC (Itasca Consulting Group, 2002) and the finite element program PLAXIS (PLAXIS BV, 2008). With numerical analyses it is possible to study other failure modes.

1.2 Aim and scope of work

In order to increase knowledge regarding failure modes in lime/cement column improved soils, a series of model tests have been performed by the Swedish Deep Stabilization Research Centre. These experiments have been carried out as shear box tests on reduced-scale models of lime/cement columns between 1999 and 2001 (Larsson, 1999; Larsson and Broms, 2000; Larsson, 2008) The aim of the present work is to simulate some of those tests with the FE program ABAQUS. Numerical analyses allow the study of several failure modes, including composite shearing, column bending and tilting, whereas limit equilibrium analyses solely consider shearing. Numerical analyses are however often oversimplified in two ways:

- They assume plain-strain condition.
- The soil and the columns are modeled as Mohr-Coulomb elasto-plastic materials.

This thesis aims to numerically reproduce the experimental tests using a three-dimensional geometry and a different material model for the columns. A review of the existing works – including the shearing tests performed by the Swedish Deep Stabilization Research Centre, which are the basis of this thesis – is presented in chapters 2 and 3. The FE program ABAQUS is then introduced and the material models and FE analyses are explained in chapter 4. The results and discussion are presented in chapter 5.

2 Laboratory tests

2.1 Procedure

The starting point of this thesis is results from the shear box tests performed by the Swedish Deep Stabilization Research Centre. The main advantages of model tests over field tests is that many uncertainties related to e.g. soil inhomogeneity, strength and deformations properties can be reduced. In the field it is very difficult to study failure mechanisms due to difficulties associated to excavations in soft soils. The main failure process is often followed by post failures that make visual observations difficult. In the laboratory, it is also possible to install measuring instruments. The preparation of kaolin, the installation of lime/cement columns, the test setup and the results are described exhaustively by Larsson (2008).

Kaolin clay

Kaolin clay was used in the tests. It is a white clay whose main mineral is kaolinite and with relatively coarse grains, with sizes between 1 μm and 40 μm . It is one of the most common materials used for model grounds because its properties are similar to natural clays, it has a relatively low cost and it is easily available. The laboratory soil was prepared by a simplified method, based on the method described by McManus and Kulhawy (1991 and 1993). Dry clay powder was mixed with tap water up to a water content of about 90 % in a concrete mixer in order to produce uniform slurry. The clay slurry was then consolidated vertically using pressurized air. The consolidation pressure was increased in stages up to 60 kPa. Single vertical drainage was allowed downwards through a 50 mm thick sand layer. The same method was used by Kitazume and Maruyama for centrifuge model tests (2006). Properties of the consolidated kaolin clay are gathered in Table 2.1.

Table 2.1: Properties of the consolidated kaolin clay.

Property	Value
Specific gravity [t/m^3]	2.6
Water content [%]	48-51
Liquid limit [%]	54
Plastic limit [%]	30
Plasticity index [%]	24
Coefficient of consolidation [m^2/s]	$3 \cdot 10^{-7}$ - $10 \cdot 10^{-7}$
Shear strength [kPa]	4-6 (drop cone test)

Lime/cement columns

The lime/cement column method is a deep mixing method using cement and lime as a binder. Columns can be installed according to two different methods, namely the dry and the wet method. In the dry method, dry binder powder transported by compressed air, is mixed in-situ with the soft soil. In the wet method cement-water slurry is mixed in-situ with the soil. The dry method is mainly used in Sweden and was chosen for the laboratory tests.

A dry mixture of lime/cement, sufficient for 100 mm of the column, was poured into a tube. The tube was then lifted 100 mm at the same time as a rod was used to maintain the binder down in the soil. This procedure was repeated until a 500 mm long string of binder was formed. Two strings were installed for each column. A mixing device with inclined paddles at three levels was rotated through the soft soil down to the bottom of the shear box. The mixing device was then withdrawn at a constant speed of 2 m/min and a constant rotational velocity of 320 rpm. This procedure was repeated three times for each column. The installation of the columns is showed in Figure 2.1.

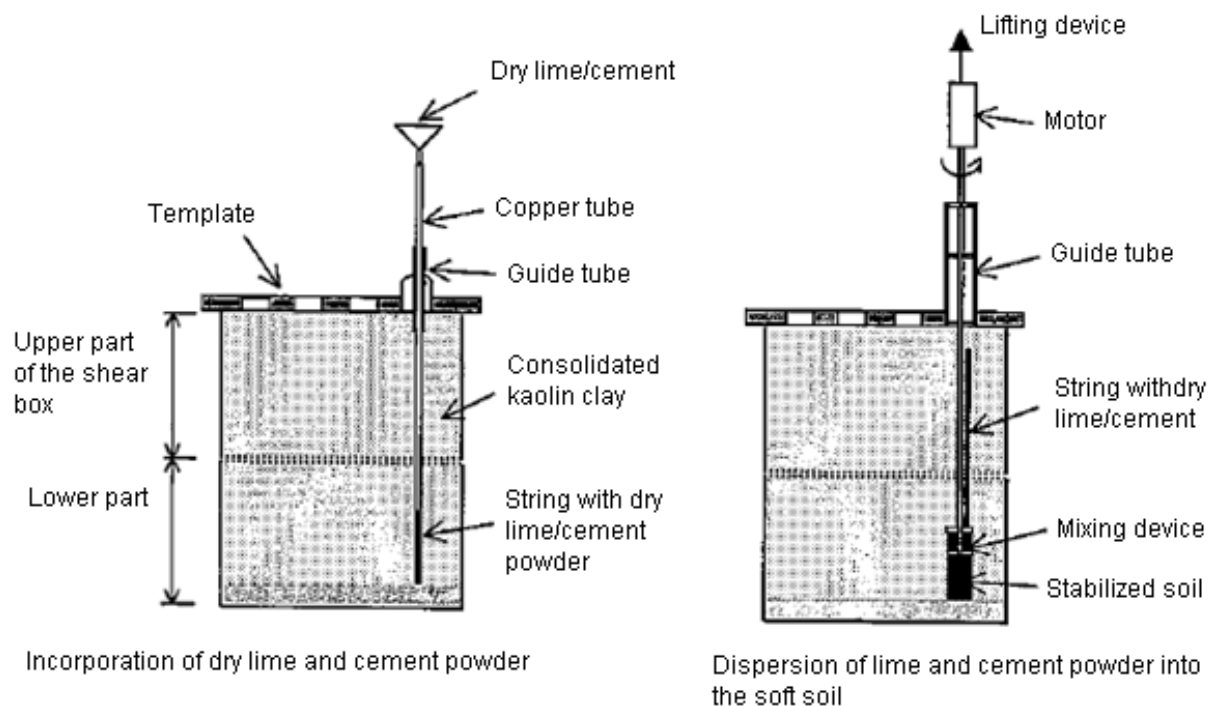


Figure 2.1: Schematic of the installation of lime/cement columns in the shear box. From Larsson (1999).

The composition of the binder was 30% lime and 70% cement, and the quantity was 150 kg/m^3 . After the columns were installed, a 50 mm thick layer of clay at the top was replaced by sand, see Figure 2.2. A normal pressure of 15 kPa was applied after one day. The shearing tests were performed two weeks after the installation of the lime/cement columns. The columns were installed with several patterns. Single columns and two rows of overlapping columns are showed in Figure 2.3. The final dimensions of the shear box and the columns are summarized in Table 2.2.



Figure 2.2: Top surface without and with a 50 mm thick sand layer. From Larsson (2008).

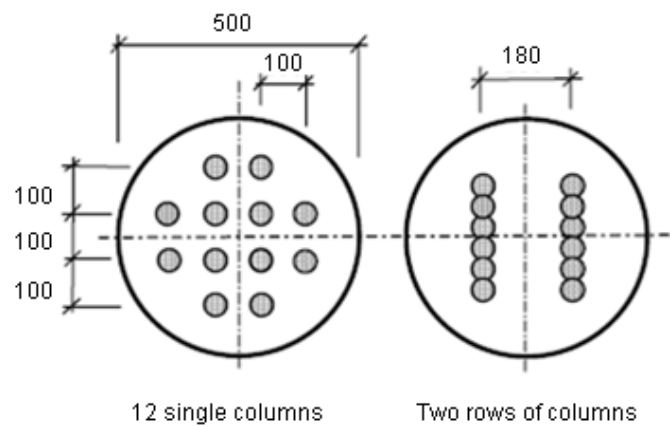


Figure 2.3: Location of the columns in the shear box. From Larsson and Broms (2000).

Table 2.2: Dimensions of the shear box apparatus.

	Column	Steel box
Diameter [mm]	50	500
Height [mm]	500	600

Shear box tests

The shear box is shown schematically in Figure 2.4, and the apparatus can be seen in Figure 2.5. The lower part of the steel barrel was fixed and the top steel plate was free to move to accommodate volume changes during the tests. The normal pressure on the steel plate was 15 kPa for the stabilized soil and 10 kPa for the unstabilized soil. The upper part of the shear box underwent a traction force. The shear stress increments were 0.64 kPa up to a level of about 4 kPa, and were then reduced to 0.32 kPa. There was one minute between two consecutive increments. The weights were applied to the box through a pulley; each increase was approximately 10 to 15 kg. The horizontal deformation of the shear-box was measured at 5, 30 and 60 seconds after each load.

A total of 23 shear tests were carried out with various configurations – single columns, overlapping columns with and without anchor and arching columns. Four of them were carried out on non-reinforced clay. The tests with stabilizing columns took from 15 to 20 minutes to carry out, and those without took from 7 to 15 minutes. This was hence a relatively quick experiment.

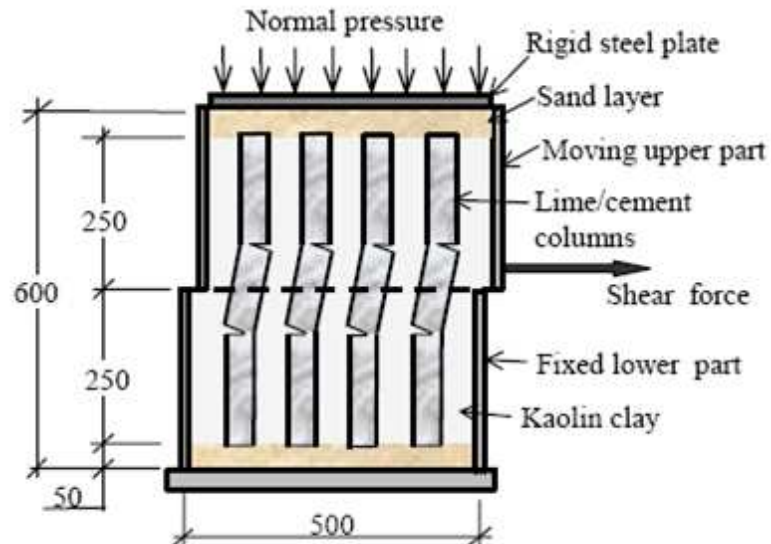


Figure 2.4: Schematic of the shear box test. From Larsson and Broms (2000).



Figure 2.5: Shear box apparatus. From Larsson (2008).

2.2 Results

The results from some of the shear box tests are showed in Figure 2.6. The configuration for each test is given in Table 2.3.

Table 2.3: Configuration for the tests.

Test	Configuration
1	Unstabilized soil
2	12 single columns
3	Two rows of columns
4	Two rows of columns
5	Two rows of columns, each row reinforced by one screw anchor

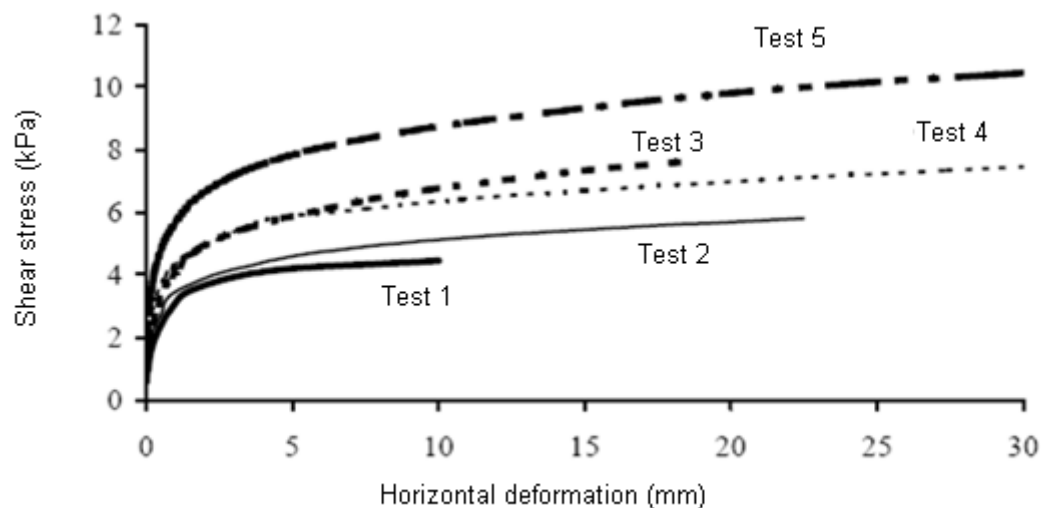


Figure 2.6: Shear resistance in the shear box tests. From Larsson and Broms (2000).

The unstabilized soil failed at a shear stress of about 4.4 kPa and a horizontal displacement of about 10 mm. Single lime/cement columns did not contribute greatly to the shear resistance (they failed at about 6 kPa and a horizontal displacement of about 18 mm), whereas overlapping columns significantly increased the shear resistance (they failed at about 8 kPa and a horizontal displacement of about 25 mm). The shear resistance was even higher when the rows of columns were reinforced with screw anchors.

Several complementary field tests were performed afterwards. For the clay the measured parameters were the water content and the undrained shear strength. The columns were exposed for the investigation of failures and crack pattern. Samples were taken for uniaxial compressive tests. The columns after shearing can be seen in Figure 2.7, for single and overlapping configuration respectively.

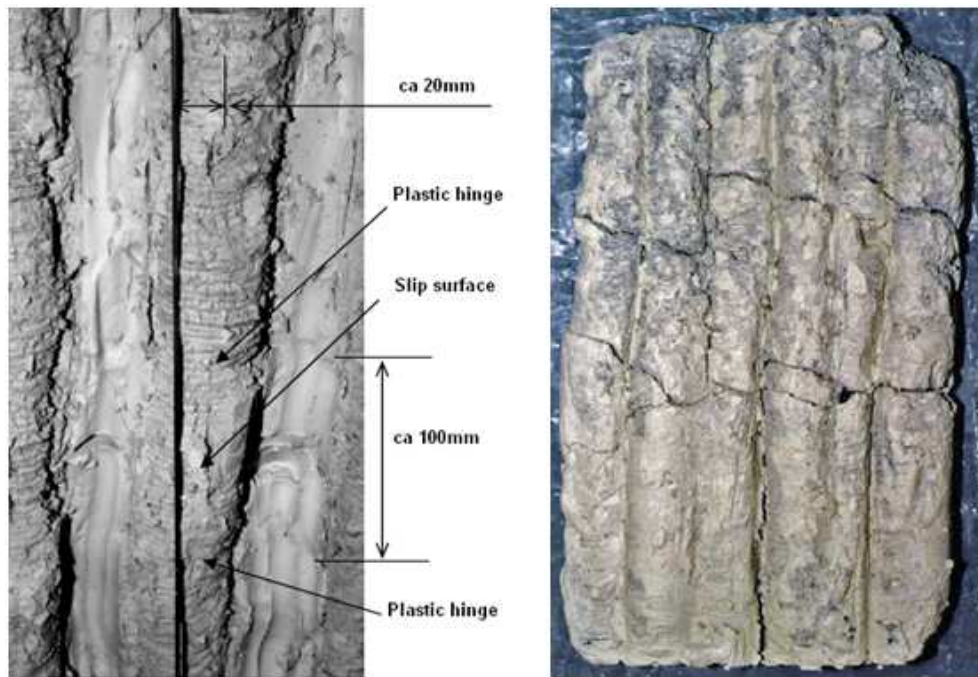


Figure 2.7: Deformed columns after the tests. From Larsson (2008).

Some of the most important observations were that:

- The clay flows around the columns.
- Plastic hinges appear for both single and overlapping columns, approximately 100 mm apart. This corresponds to a bending failure, that is, the columns fail when the moment capacity is exceeded.
- The cracks resemble those in concrete.

3 Review of previous work

3.1 Design methods

The current Swedish design method considers the stabilized soil as a composite material (SGF, 2000; Vägverket, 2009). The peak shear strength of the columns is mobilized at the same time as the peak shear strength of the unstabilized soil between the columns, see Figure 3.1. This means that there is full interaction between the soil and the columns. Failure is assumed to occur along a slip surface through the columns and the surrounding soil.

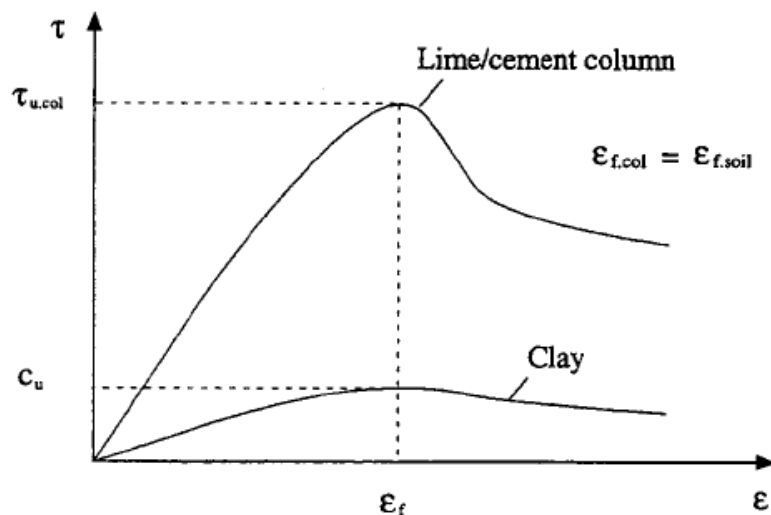


Figure 3.1: Assumed strains in the calculation of weighted average shear strength. From Kivelö (1998).

A weighted average undrained shear strength of the stabilized soil is used to estimate the stability:

$$c_u = c_{u,col} \cdot a + c_{u,clay} \cdot (1 - a)$$

where,

$c_{u,col}$ is the undrained shear strength of lime/cement. It is practically assumed to be half of the unconfined compressive strength.

$c_{u,clay}$ is the undrained shear strength of clay.

a is the area ratio of the columns (column area/total area).

According to the Swedish design code a combined shear strength should also be considered (the lowest value of drained and undrained strength of each component).

The Swedish design code gives also guidelines to estimate the stress distribution caused by a vertical load, typically the weight of the embankment. If q_n is the normal load over the total area, i.e. soil and columns, the stress increase within a column is:

$$\sigma_{col} = \frac{q_n}{a + \frac{M_{clay}}{E_{col}}(1 - a)}$$

where,

E_{col} is the modulus of elasticity of the lime/cement columns.

M_{clay} is the odometer modulus of the clay.

The design method in Japan (CDIT, 2002) is similar, in that it considers the stabilized soil as a composite material. However, unlike the Swedish practice, it assumes that the shear strengths of the columns and the unstabilized soil between the columns are not mobilized at the same time. The axial strain at the peak shear strength of the lime/cement column is small compared with the failure strain of the undisturbed clay, see Figure 3.2. When the peak shear strength of the soft clay is exceeded, the shear strength of the columns has already decreased to a residual value. The small failure strain of the lime/cement columns will reduce the interaction with the unstabilized soil.

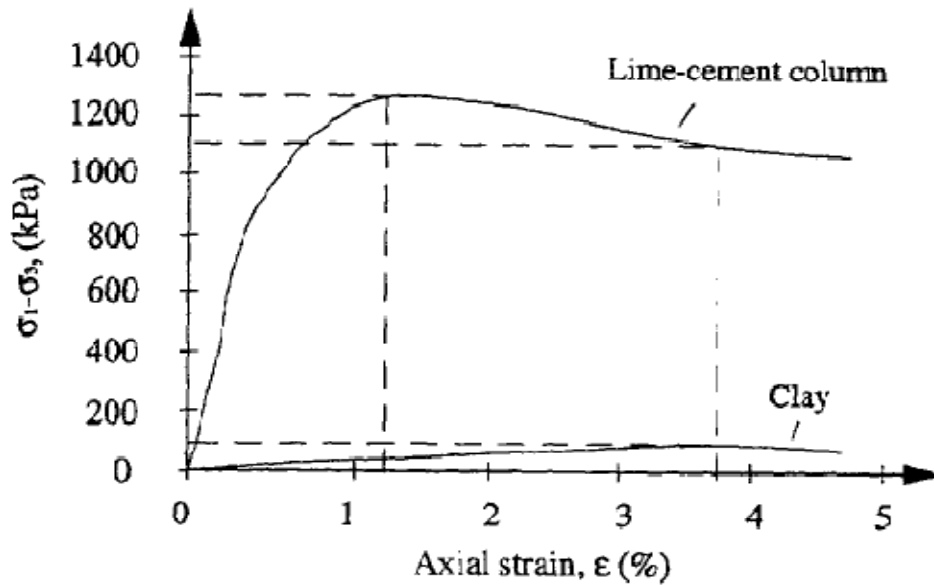


Figure 3.2: Stress-strain curves of lime/cement columns and of unstabilized clay. From Kivelö (1998).

Design methods in Scandinavia, Japan and the US estimate the stability of reinforced embankments with limit equilibrium analyses. Two failure patterns, referred to as *internal* and *external* stabilities and showed in Figure 3.3, are studied:

- For the internal stability, columns are assumed to fail by shearing. The stability is studied through a slip circle analysis, which means that all the columns fail at the same time regardless of their location.
- For the external stability, the columns and clay between are assumed to fail by sliding. The reinforced soil moves horizontally without any rearrangement of columns.

This is basically identical to Bishop's method for unstabilized ground. Limit equilibrium slope stability analyses are performed assuming a slip circle failure on which the shear stress exceeds the shear strength of the soil (which is here the weighted average shear strength of the columns and the unstabilized soil). Several slip surfaces are tested and the most probable is the one that gives the lowest factor of safety. Computer programs such as UTEXAS4 (Wright, 1999) are commonly used.

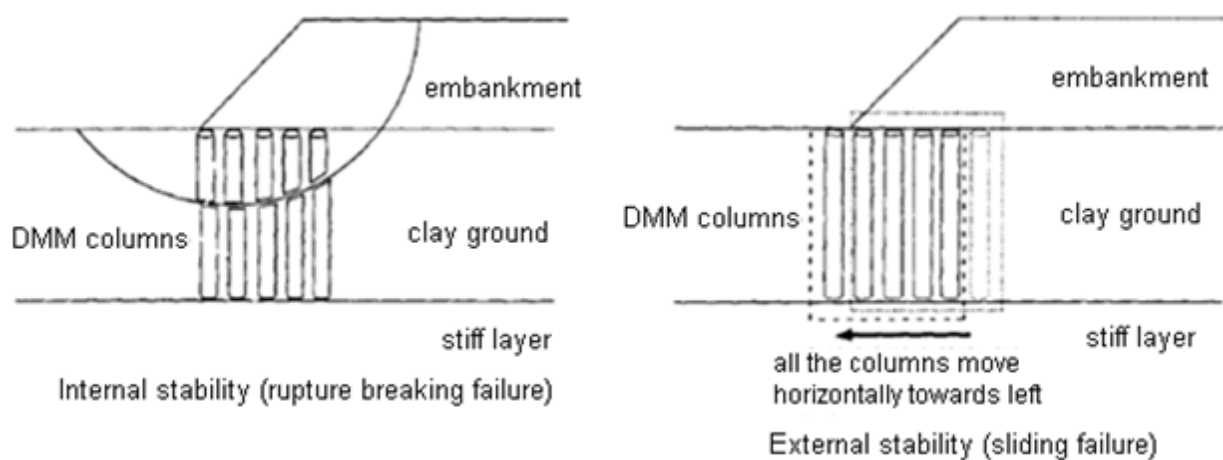


Figure 3.3: Assumed failure patterns of DM improved grounds in the current design method. From Kitazume and Maruyama (2006).

3.2 Limitations of the design methods

According to the Swedish design method the undrained shear strength is calculated as the weighted average of the undrained shear strengths of lime/cement columns and kaolin clay. These are in the present study estimated as 60 kPa and 4.4 kPa respectively. The area ratio is 12 % for single columns and 11 % for two rows of columns. The shear strength of the stabilized soil is then 11 kPa for single columns. This value is much higher than the experimental value of 6 kPa (see Figure 2.6), i.e. the current design method overestimates the shear strength and the stability of the reinforced soil.

Previous work including centrifuge model tests (Kitazume et al., 2006 and 2009), numerical analyses (Adams et al. 2009, Han et al. 2005, Kitazume et al. 2006 and 2009) and theoretical research (Kivelö, 1998) has showed that the shear failure and the sliding failure modes are not the most probable modes for internal and external stability respectively. Numerical analyses are more powerful than limit

equilibrium slope analyses because they are able to take other failure modes than shear into account, namely bending, tilting and racking.

Adams et al. (2009) used the finite difference program FLAC (Itasca Consulting Group, 2002) to study the internal stability (failure of the columns under embankment load) of single columns and shear walls. Several important conclusions can be drawn:

- Numerical analyses give a lower factor of safety than limit equilibrium slope analyses do. This means that considering solely shear failure overestimates the embankment stability (the classical methods tend to be unconservative).
- Single columns fail with a failure bending mode. This behavior is proposed by Kivelö (1998) and confirmed by the tests performed by Larsson (1999 and 2008) and Larsson and Broms (2000).
- DMM shear walls are more effective than single columns at the same area replacement ratio, i.e. about the same cost for raw material. The same conclusion was drawn by Larsson (2008).
- The failure modes of shear walls are greatly influenced by the interaction between the overlapping columns. If the interaction is assumed to be complete (that is, the compressive strength of the material between two columns is equal to the compressive strength of the columns), then the shear wall fails by sliding and shearing. In reality the mixing process of the columns leads to weaker joints between the overlapping columns. When the vertical joint efficiency is below 30% of the strength of the columns, the shear walls fail by racking. The same behavior is indicated by the test performed by Larsson (2008), where the overlapping distance between the columns was varied.

Han et al. (2005) compared the results obtained with FLAC with those obtained with Bishop's method. They varied several parameters, such the size and strength of the columns, the spacing between them, the thickness of the soft soil underneath. In all configurations Bishop's method gave factors of safety higher than with FLAC. They also concluded that failure of the columns was more probably bending and rotation instead of shearing.

Kitazume et al. (2006 and 2009) studied external and internal stability of single columns via centrifuge model tests and numerical analyses using PLAXIS (PLAXIS BV, 2008). Their results regarding internal stability are in agreement with Adams et al. results (2009): the columns fail one by one in the bending failure mode in sequence from the forefront to the rearmost column (Figure 3.4). For the external stability, failure by sliding – as assumed in the design methods – occurs only under certain conditions (when the shear strength of the clay ground decreases with depth or when the columns penetrate partially in the clay ground). Otherwise, improved embankments fail with a collapse failure pattern, that is, the columns tilt like dominos at the bottom, see Figure 3.5.

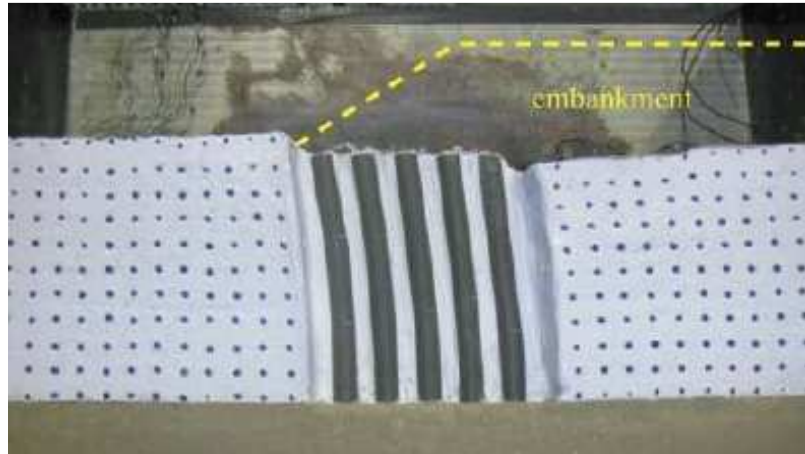


Figure 3.4: Column failure. From Kitazume et al. (2009).

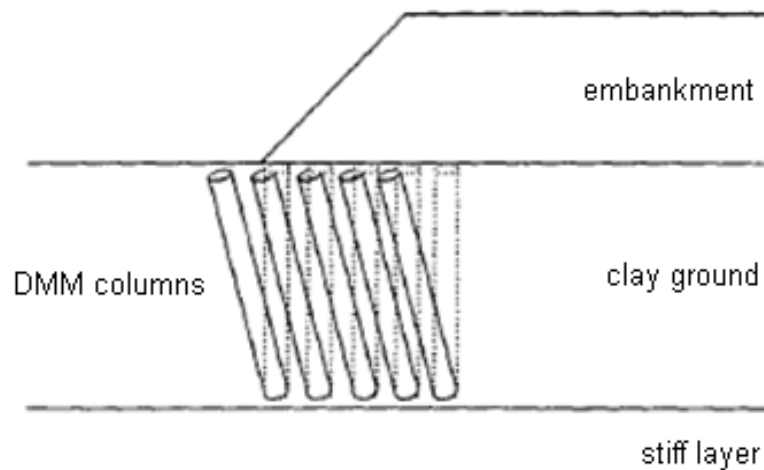


Figure 3.5: Collapse failure pattern of DM improved ground. From Kitazume et al. (2009).

Kivelö (1998) identified and analyzed several failure modes:

- The moment capacity of the columns is exceeded, leading to plastic hinges (their amount and location depend on the location of the columns under the embankment).
- The lateral resistance of the unstabilized soil is exceeded (the soil flows around the columns).
- The shear strength or the compressive strength of the columns is exceeded.

The moment capacity of lime/cement columns is strongly affected by the axial load and reaches its maximum when the axial load is half the ultimate load. A plastic hinge develops below the slip surface where the maximum bending moment exceeds the

moment capacity of the column (this failure occurs when the depth of the sliding soil mass above the slip surface is small compared with the length of the columns). The upper part of the column will rotate around the plastic hinge. When the depth of the sliding mass reaches about the middle of the columns, as is the case in the reduced-scale tests, a second plastic hinge develops above the slip surface. One reason for which bending failure of single columns is more probable than shear failure is that when the columns have a relatively high shear strength and stiffness compared with the surrounding clay, high bending moments can be developed.

4 Finite Element analyses

4.1 The Finite Element Program ABAQUS

ABAQUS is a general-purpose, production oriented finite element program designed for advanced analysis of engineering problems. It is developed by Dassult Systèmes/SIMULIA. It can be used to solve a wide variety of problems and modeling of many geometrics and material behaviors. It consists of two main analysis products – ABAQUS/Standard (SIMULIA, 2009) and ABAQUS/Explicit (SIMULIA, 2009):

- ABAQUS/Standard is a general-purpose analysis product that can solve a wide range of linear and nonlinear problems involving the static, dynamic, thermal, and electrical response of components.
- ABAQUS/Explicit is a special purpose analysis module for solving explicit dynamic analyses and also quasi-static analyses if the load is applied very slowly.

All the numerical simulations presented in this thesis were performed using ABAQUS/Standard.

A complete ABAQUS analysis usually consists of three distinct stages: preprocessing, simulation, and postprocessing. In the preprocessing stage the model of the physical problem is defined by creating an ABAQUS input file. The model is usually created graphically using ABAQUS/CAE (SIMULIA, 2009) or another preprocessor, although the ABAQUS input file for a simple analysis can be created directly using a text editor. The simulation is the stage in which ABAQUS/Standard or ABAQUS/Explicit solves the numerical problem defined in the model; it is normally run as a background process. Depending on the complexity of the problem being analyzed and the computer power, it may take anywhere from seconds to days to complete an analysis run. In the present case the simulations took from several hours to several days. The last stage is the postprocessing, generally done interactively using the Visualization module of ABAQUS/CAE or another postprocessor. The Visualization module, which reads the neutral binary output database file, has a variety of options for displaying the results, including color contour plots, animations, deformed shape plots, and X–Y plots. These three stages are linked together by files, see Figure 4.1.

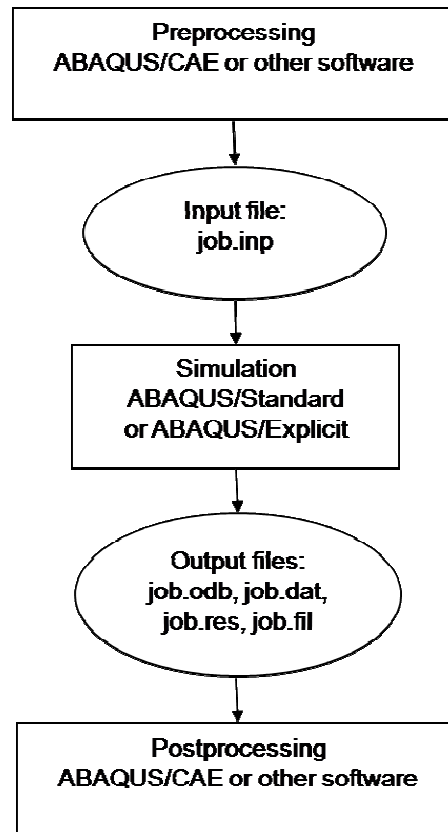


Figure 4.1: Different stages involved in a complete ABAQUS analysis.
From ABAQUS 6.6 (2009).

4.2 Material modeling in ABAQUS

4.2.1 Brief summary of continuum mechanics

Most plastic models and failure criteria are isotropic, that is, they are independent of material orientation and the coordinate system used (Chen, 1994). Hence the yield function and the flow potential can be represented in terms of the principal stresses $(\sigma_1, \sigma_2, \sigma_3)$, or the stress invariants (I_1, J_2, J_3) , or scaled versions of the invariants. The stress deviator is defined as $\mathbf{s} = \boldsymbol{\sigma} + p\mathbf{I}$. I_1 is the first invariant of the stress tensor $\boldsymbol{\sigma}$, J_2 and J_3 are the second and third invariants of \mathbf{s} .

$$I_1 = \boldsymbol{\sigma} \cdot \mathbf{I} = \text{Tr}(\boldsymbol{\sigma}) = \sigma_1 + \sigma_2 + \sigma_3$$

$$J_2 = \frac{1}{2} \mathbf{s} : \mathbf{s} = \frac{1}{6} [(\sigma_1 - \sigma_2)^2 + (\sigma_2 - \sigma_3)^2 + (\sigma_3 - \sigma_1)^2]$$

$$J_3 = \det(\mathbf{s}) = \frac{1}{3} (\mathbf{s} \cdot \mathbf{s}) : \mathbf{s} = s_1 s_2 s_3$$

where (s_1, s_2, s_3) are the principal values of the stress deviator.

The quantities (p, q, r) are often used:

$$p = -\frac{I_1}{3} \quad (\text{hydrostatic pressure stress})$$

$$q = \sqrt{3J_2} \quad (\text{Mises equivalent stress})$$

$$r = 3\left(\frac{J_3}{2}\right)^{\frac{1}{3}}$$

Sometimes the quantities (ξ, ρ, θ) are preferred. They describe a cylindrical coordinate system (the Haigh-Westergaard coordinates), as:

$$\xi = \frac{1}{\sqrt{3}}I_1 = \sqrt{3}p$$

$$\rho = \sqrt{2J_2} = \sqrt{\frac{2}{3}}q$$

$$\cos(3\theta) = \left(\frac{r}{q}\right)^3 = \frac{3\sqrt{3}}{2} \frac{J_3}{J_2^{3/2}} \quad (\theta \text{ is the Lode angle})$$

4.2.2 Lime/cement improved kaolin

In most FE analyses both lime/cement and clay are modeled as Mohr-Coulomb elasto-plastic materials. The plastic behavior of lime/cement is here modeled with the concrete damaged plasticity model. This model has been successfully used to describe cracking of concrete, see e.g. Malm (2009).

Linear elastic behavior

Before undergoing plastic deformation and damage, the behavior of lime/cement can be modeled as linear elastic. Young's modulus is here determined from uniaxial compressive tests (see below), and Poisson's ratio is assumed to be 0.15. The basic properties of lime/cement are gathered in Table 4.1.

Table 4.1: Basic mechanical properties of lime/cement.

Property	Value
Density [kg/m ³]	1500
Elastic modulus [MPa]	20
Poisson's ratio	0.15

The concrete damaged plasticity model

As seen previously, the crack pattern in lime/cement columns displays similarities with concrete, which is the reason for using a concrete model – the concrete damaged plasticity model – to simulate lime/cement, even though it is a much more brittle and weaker material. This model is primarily intended for the analysis of reinforced concrete under fairly low pressures and cyclic loading, but it can also be used for quasi-brittle materials such as mortar, rocks and ceramics, since concrete behaves in a brittle manner under low confining pressures. It is based on the models proposed by Lubliner et al. (1989) and by Lee and Fenves (1998). The concrete damaged plasticity model in ABAQUS (SIMULIA, 2009) consists of a combination of non-associated multi-hardening plasticity and isotropic damaged elasticity.

Uniaxial tensile behavior

The uniaxial tensile behavior is illustrated in Figure 4.2. The stress-strain response is linear elastic until the failure stress σ_{t_0} is reached. The plastic behavior displays strain softening, corresponding to the formation of micro-cracks. In the model, damages in the material are accounted for through an isotropic reduction of the elastic stiffness. When the material is unloaded from any point on the strain softening branch, the elastic stiffness is degraded. The stress-strain relationship under uniaxial tension is:

$$\sigma_t = (1 - d_t)E_0(\varepsilon_t - \tilde{\varepsilon}_t^{pl})$$

where,

$\tilde{\varepsilon}_t^{pl}$ is the equivalent plastic strain in tension,

E_0 is the initial (undamaged) elastic stiffness of the material, and

d_t is the damage variable in tension.

The evolution of d_t depends on the plastic strain ($d_t = d_t(\tilde{\varepsilon}_t^{pl})$); the effect is more pronounced as the plastic strain increases. It can take values in the range from zero (undamaged material) to one (fully damaged material). Stiffness degradation is thus isotropic. The effective tensile cohesion stress is defined as:

$$\bar{\sigma}_t = E_0(\varepsilon_t - \tilde{\varepsilon}_t^{pl}) = \frac{\sigma_t}{(1 - d_t)}$$

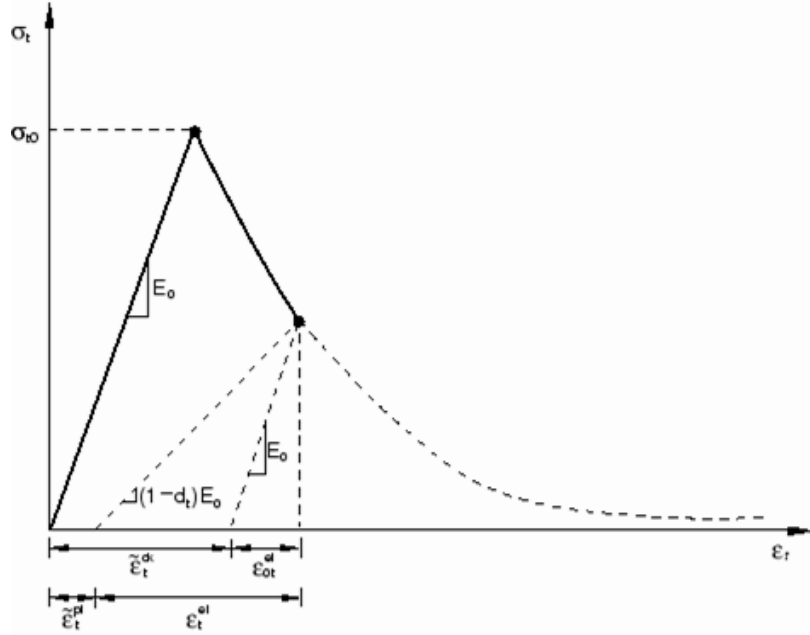


Figure 4.2: Response of concrete to uniaxial loading in tension.
From ABAQUS 6.6 (2009).

The specification of postfailure behavior in uniaxial tension means giving the postfailure stress as a tabular function of either (1) the cracking strain ε_t^{ck} , (2) the cracking displacement u_t^{ck} , (3) the fracture energy G_f . The strain softening branch is hence defined as a succession of linear functions. Defining the strain softening branch with the cracking displacement should be avoided in cases with no reinforcement because it can induce mesh sensitivity related problems.

The fracture energy cracking model is preferably used to specify the postfailure stress as a function of cracking displacement. The fracture energy is the energy required to open a unit area of crack (Hillerborg, 1976). It is related to the failure stress σ_{t0} and the final cracking displacement u_{t0} , at which complete loss of strength takes place, through the relationship:

$$G_f = \frac{\sigma_{t0} \cdot u_{t0}}{2}$$

This is the area under the postfailure stress-displacement curve, see Figure 4.3.

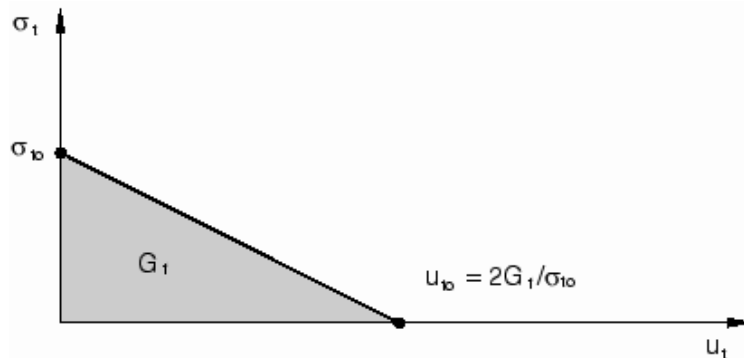


Figure 4.3: Postfailure stress-fracture energy curve. From ABAQUS 6.6 (2009).

According to the ABAQUS manual a typical value of G_f for an average quality concrete with a compressive strength of 20 MPa is 40 N/m (or J/m²). Since lime/cement is a much weaker and more brittle material than concrete a lower value of the fracture energy was assumed as $G_f = 10$ N/m. The tensile yield stress is assumed to be a fraction of the compressive strength (described after). It is taken as $\sigma_{t_0} = 8$ kPa and the final cracking displacement is then $u_{t_0} = 0.00245$ m. The strain softening curve is defined simply as a single linear function (Table 4.2).

Table 4.2: Strain softening values.

Tensile yield stress [kPa]	Cracking displacement [m]
8	0
0.16	0.00245

As plastic deformations increase, the material is damaged through reduction of its stiffness. This reduction increases itself with increasing deformations. d_t is specified as a tabular function of u_t^{ck} . If not, the model behaves as a simple plasticity model i.e. no damage occurs. Incorrect damage curves cause errors in plastic strains computations if the plastic strain values are negative and/or decreasing with increasing cracking strain. The highest value giving positive plastic strain is chosen (see Table 4.3).

Table 4.3: Tensile damage parameter values.

Tensile damage parameter	Cracking displacement [m]
0	0
0.99	0.00245

ABAQUS automatically converts the cracking displacement values to “plastic” displacement values using the relationships:

$$u_t^{pl} = u_t^{ck} - \frac{d_t}{1 - d_t} \frac{\sigma_t l_0}{E_0}$$

$$u_t^{ck} = \tilde{\epsilon}_t^{ck} \cdot l_0$$

where l_0 is assumed to be one unit length. The uniaxial stress-strain curve in tension is then completely defined. As knowledge regarding fracture energy and tensile yield stress of lime/cement is rare, these properties have been derived from the values commonly used for concrete. This choice is then “arbitrary”, in the sense that other choices of fracture energy/tensile yield stress have also been tried and have led to similar results. This is further discussed in section 5.2.

Uniaxial compressive behavior

The uniaxial compressive behavior is illustrated in Figure 4.4. As in uniaxial tension the behavior is linear elastic up to the initial yield stress σ_{c0} , but the plastic response displays both stress hardening and strain softening. Damages are defined in the same way as in uniaxial tension. When the material is unloaded from any point on the strain softening branch, the elastic stiffness is isotropically degraded.

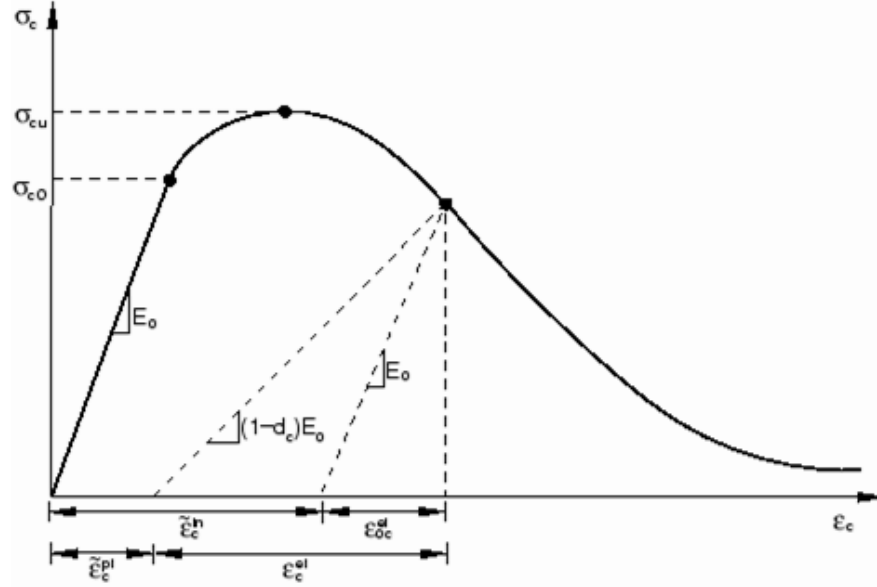


Figure 4.4: Response of concrete to uniaxial loading in compression.
From ABAQUS 6.6 (2009).

The stress-strain relationship under uniaxial compression loading is:

$$\sigma_c = (1 - d_c)E_0(\varepsilon_c - \tilde{\varepsilon}_c^{pl})$$

where $\tilde{\varepsilon}_c^{pl}$ is the equivalent plastic strain in compression. The degradation of the elastic stiffness is characterized by the second damage variable d_c . The effective compressive cohesion stress is defined as:

$$\bar{\sigma}_c = E_0(\varepsilon_c - \tilde{\varepsilon}_c^{pl}) = \frac{\sigma_c}{(1 - d_c)}$$

Similar to tension, the stress-strain behavior in uniaxial compression outside the elastic range (hardening and softening) is defined as a succession of straight lines. The yield stress σ_c is here defined as a tabular function of the inelastic strain, instead of the plastic strain. The inelastic strain is:

$$\tilde{\varepsilon}_c^{in} = \varepsilon_c - \varepsilon_{0c}^{el}$$

where,

ε_c is the total strain, and

$\varepsilon_{0c}^{el} = \sigma_c/E_0$ is the elastic strain corresponding to the undamaged material.

The columns were excavated after the tests, and then uniaxial unconfined compressive tests were performed on small samples (Figure 4.5). The strain rate was 0.5 mm/min. The unconfined compressive strength is about 120 kPa. The strain-stress curves are quite similar to that of concrete, with a larger plastic zone. However the results are very scattered. Such uncertainties have previously been considered in numerical analyses: Adams et al. (2009) assigned a coefficient of variation of 50% to the column strength. Inhomogeneities within the lime/cement columns should also be considered. For instance, the diameter of the columns increased slightly with the depth, probably due to the mixing device, and the columns were stronger in the upper part than in the lower part of the shear box. That is why lower strength properties than those indicated by the tests have been chosen. Both curves are showed in Figure 4.6. The values that are used in the FE analyses are showed in Table 4.4.



Figure 4.5: Samples before the unconfined compression tests. From Larsson (2008).

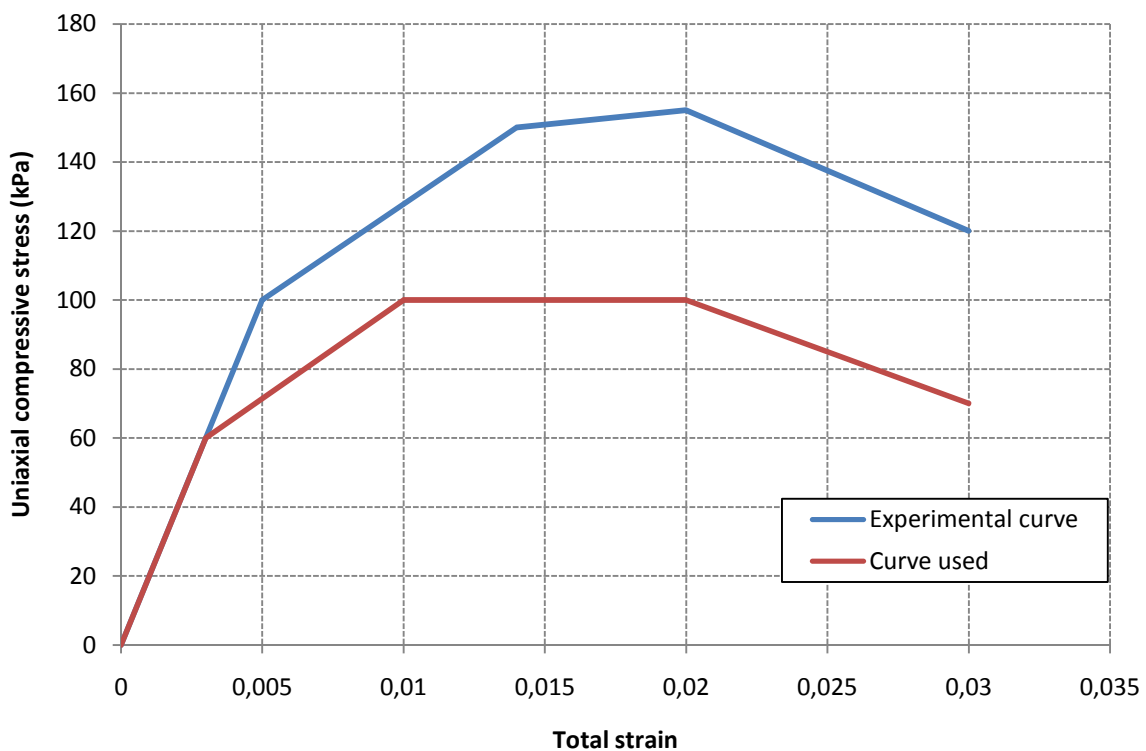


Figure 4.6: Experimental and used responses of lime/cement to uniaxial loading in compression.

Table 4.4: Uniaxial stress-strain values.

Uniaxial compressive stress (kPa)	Total strain	Inelastic strain
0	0	0
60	0.003	0
100	0.01	0.007
100	0.02	0.017
70	0.03	0.027

Compressive damage (crushing of the material) was also considered. The compressive damage parameter d_c is defined as a tabular function of $\tilde{\varepsilon}_c^{in}$. Little degradation of the stiffness is assumed to happen due to compressive stresses before strain softening. ABAQUS automatically converts the inelastic strain values to plastic strain values using the relationship:

$$\tilde{\varepsilon}_c^{pl} = \tilde{\varepsilon}_c^{in} - \frac{d_c}{1 - d_c} \frac{\sigma_c}{E_0}$$

The calculated plastic strain values must be positive and increasing with increasing inelastic strain. The final value of d_c is chosen as the maximal value according to this condition (see Table 4.5).

Table 4.5: Compressive damage parameter values.

Compressive damage parameter	Inelastic strain
0	0
0.05	0.007
0.1	0.017
0.75	0.027

Uniaxial cyclic behavior

The behavior of concrete under uniaxial cyclic loading (alternation of tensile and compressive loadings) is quite complex. The stiffness recovery is different depending on the order of the loadings. Similar to the uniaxial tensile and compressive behaviors, the stiffness degradation is isotropic and described by a scalar degradation variable d as $E = (1 - d)E_0$. The variable d is defined from the uniaxial damage variables in tension and compression:

$$(1 - d) = (1 - s_t d_c)(1 - s_c d_t)$$

where s_t and s_c depend on the weight factors w_t and w_c . These factors control the recovery of the tensile and compressive stiffness upon load reversal and are assumed to be material properties.

Experimental observations in most quasi-brittle materials show that the compressive stiffness is recovered upon crack closure as the load changes from tension to compression ($w_c = 1$). On the other hand, the tensile stiffness is not recovered as the

Yield function

The yield function F determines under which state of stress plastic deformations occur. The state of stress inside the yield surface ($F < 0$) is elastic. When the stresses lie on the surface ($F = 0$) the material has reached its yield point and becomes plastic. Further deformation causes the stress state to remain on the yield surface, even though the surface itself may change shape and size as the plastic deformation evolves (hardening and/or softening). Stress states outside the yield surface ($F > 0$) are physically non-permissible. For a one-dimensional state of stress the yield function can easily be defined in terms of the uniaxial tensile strength. Under multiaxial states of stress the yield function is defined in terms of the stress invariants.

The yield function used in ABAQUS is a combined geometric shape of two different Drucker-Prager type functions. It was developed by Lubliner et al. (1989) and includes the modifications proposed by Lee and Fenves (1998) to account for different evolutions of strength under tension and compression (Figure 4.8). It is expressed as:

$$F(\bar{\boldsymbol{\sigma}}, \bar{\boldsymbol{\varepsilon}}^{pl}) = \frac{1}{1-\alpha} (\bar{q} - 3\alpha\bar{p} + \beta(\bar{\boldsymbol{\varepsilon}}^{pl})\langle\hat{\sigma}_{max}\rangle - \gamma\langle-\hat{\sigma}_{max}\rangle) - \bar{\sigma}_c(\bar{\boldsymbol{\varepsilon}}_c^{pl})$$

where the Macauley bracket is defined by $\langle x \rangle = \frac{1}{2}(|x| + x)$, i.e. $\langle x \rangle = x$ if $x > 0$ and $\langle x \rangle = 0$ if $x < 0$.

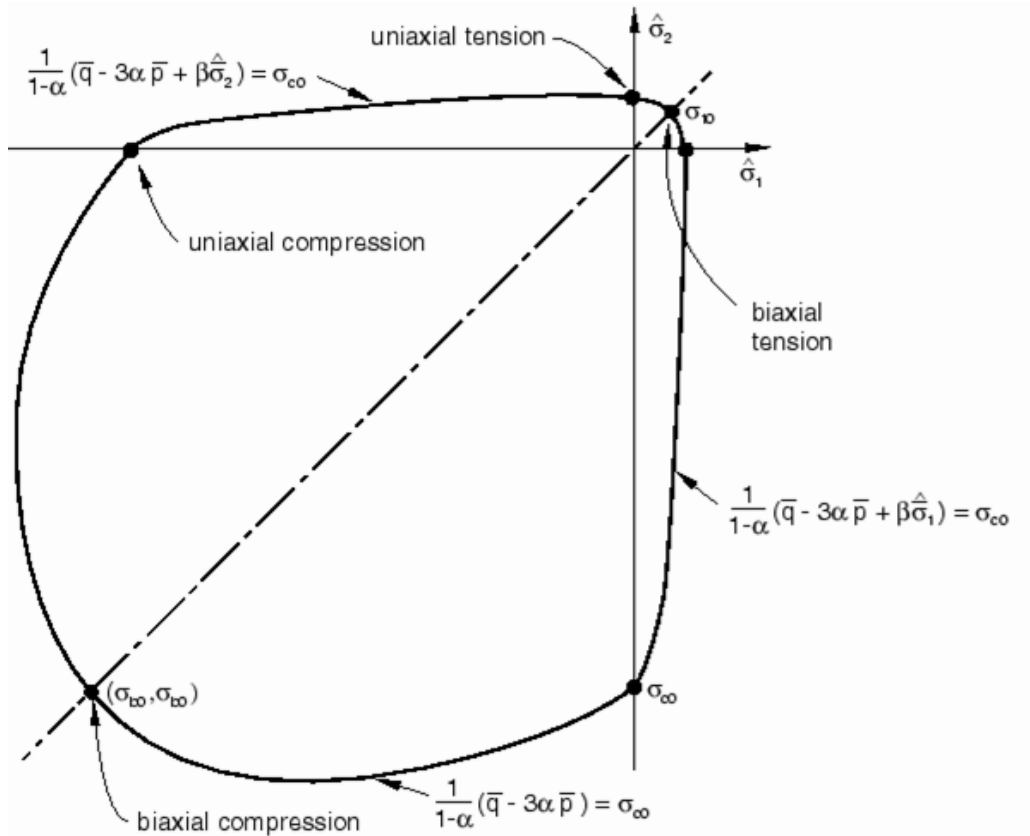


Figure 4.8: Yield surface in plane stress. From ABAQUS 6.6 (2009).

The parameters are:

$$\alpha = \frac{(\sigma_{b0}/\sigma_{c0}) - 1}{2(\sigma_{b0}/\sigma_{c0}) - 1}; 0 \leq \alpha \leq 0.5$$

$$\beta = \frac{\bar{\sigma}_c(\tilde{\varepsilon}_c^{pl})}{\bar{\sigma}_t(\tilde{\varepsilon}_t^{pl})}(1 - \alpha) - (1 + \alpha)$$

$$\gamma = \frac{3(1 - K_c)}{2K_c - 1}$$

where,

$\hat{\sigma}_{max}$ is the maximum principal effective stress,

σ_{c0} is the initial uniaxial compressive yield stress, and

σ_{b0} is the initial equibiaxial compressive yield stress. The default value for the ratio is used, $\sigma_{b0}/\sigma_{c0} = 1.16$. As it is superior to 1.0 this corresponds to increasing strength under biaxial states of stresses, compared to uniaxial behavior.

$\bar{\sigma}_t(\tilde{\varepsilon}_t^{pl})$ the effective tensile cohesion stress.

$\bar{\sigma}_c(\tilde{\varepsilon}_c^{pl})$ the effective compressive cohesion stress. The last parameter

K_c is the ratio of the second stress invariant on the tensile meridian, $q_{(TM)}$, to that on the compressive meridian, $q_{(CM)}$, at initial yield for any given value of the pressure invariant p such that the maximum principal stress is negative, $\hat{\sigma}_{max} < 0$. It must satisfy the condition $0.5 \leq K_c \leq 1.0$, and the default value is here used, $K_c = 2/3$. The corresponding default value of γ is 3. It enters the yield function only for stress states of triaxial compression, which means that this coefficient describes triaxial compression.

Flow rule

The plastic strain increment at yield is defined through a flow rule (normality principle):

$$d\varepsilon^{pl} = d\lambda \frac{\partial G(\bar{\sigma})}{\partial \bar{\sigma}}$$

where $d\lambda$ is a non-negative scalar called the plasticity multiplier. The plastic flow potential used in ABAQUS is the Drucker-Prager hyperbolic function (Figure 4.9):

$$G = \sqrt{(\varepsilon\sigma_{t0} \tan \psi)^2 + \bar{q}^2} - \bar{p} \tan \psi$$

where,

ψ is the dilation angle measured in the \bar{p} - \bar{q} plane (effective meridional plane) at high confining pressure. The value $\psi = 1^\circ$ is chosen.

ε is the eccentricity. It defines the rate at which the function approaches the asymptote (the flow potential tends to a straight line as the eccentricity tends to zero). The default value is used ($\varepsilon = 0.1$).

The uniaxial tensile stress at failure is taken from the user-specified tension stiffening data:

$$\sigma_{t0} = \sigma_t|_{\varepsilon_t^{pl}=0}$$

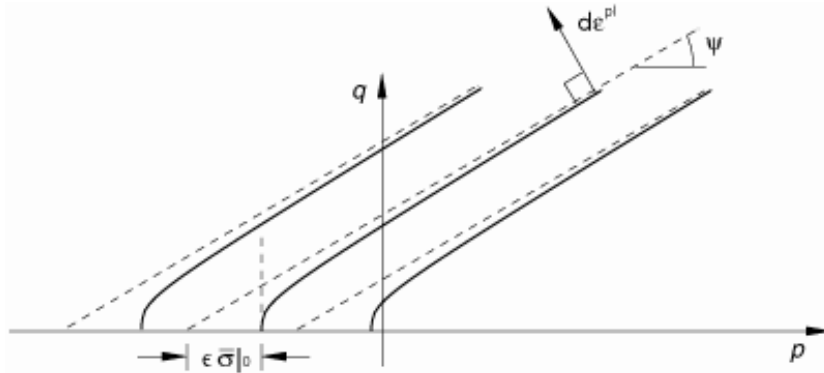


Figure 4.9: The Drucker-Prager hyperbolic plastic potential function in the meridional plane. From ABAQUS 6.6 (2009).

4.2.3 Clay

Linear elastic behavior

Prior to plastic behavior and failure, the clay is assumed to have a linear elastic response. The laboratory shearing tests performed on unstabilized soil (Larsson, 2008) were numerically reproduced in order to adjust Young’s modulus and Poisson’s ratio. The procedures and results for these numerical simulations are presented in section 5.1. The conclusion from this numerical investigation is that the properties in Table 4.6 should be used for the studied clay.

Table 4.6: Basic mechanical properties of the clay.

Property	Value
Density [kg/m ³]	1500
Elastic modulus [MPa]	0.5 - 1
Poisson’s ratio	0.45 - 0.48

Mohr-Coulomb elasto-plastic model

The Mohr-Coulomb failure criterion has been widely used for geotechnical applications, particularly in similar FE analyses, see e.g. Kitazume and Maruyama (2006). The clay is here modeled as a Mohr-Coulomb elasto-plastic material. In ABAQUS the Mohr-Coulomb plasticity model is an extension of the classical failure criterion. According to the classical model, failure occurs when the shear stress on any point in a material reaches a value that depends linearly on the normal stress in the same plane. Hence it can be written as:

$$\tau = c + \sigma \cdot \tan \varphi$$

where,

- τ is the shear stress on the failure plane,
- σ is the normal stress on the failure plane (positive in compression),
- c is the cohesion of the material, and
- φ is the angle of internal friction.

This can alternatively be written as a function of the minor (σ_3) and major (σ_1) principal stresses:

$$\frac{\sigma_1 - \sigma_3}{2} = c \cdot \cos \varphi + \frac{\sigma_1 + \sigma_3}{2} \sin \varphi$$

Or again:

$$\sigma_1 = \frac{2c \cdot \cos \varphi}{1 - \sin \varphi} + \frac{1 + \sin \varphi}{1 - \sin \varphi} \sigma_3$$

Thus, unlike the Drucker-Prager criterion, the Mohr-Coulomb criterion assumes that failure is independent of the value of the intermediate principal stress (σ_2), which is considered to be sufficiently accurate for most applications.

Yield function

ABAQUS uses a yield function of the Mohr-Coulomb form that includes isotropic cohesion hardening and/or softening. Figure 4.10 shows the yield function in the meridional plane. For general states of stress the yield function can be written in terms of three stress invariants:

$$F = R_{mc}q - p \cdot \tan \varphi - c$$

where R_{mc} is the Mohr-Coulomb deviatoric stress measure. Isotropic hardening and/or softening can be taken into account through the evolution of the cohesion as plastic deformations increase, $c = c(\varepsilon^{pl})$, where ε^{pl} is the plastic strain. The cohesion yield stress is thus defined as a tabular function of ε^{pl} , and the first value must correspond to no plastic strain. ABAQUS converts automatically the plastic strain to the equivalent plastic strain $\bar{\varepsilon}^{pl} = \int \frac{1}{c} \boldsymbol{\sigma} : d\boldsymbol{\varepsilon}^{pl}$ (an equivalent definition is $c\bar{\varepsilon}^{pl} = \boldsymbol{\sigma} : \boldsymbol{\varepsilon}^{pl}$).

Measures on unreinforced soil samples indicate that the undrained shear strength of the clay is $c_{u,clay} = 4$ kPa. Consequently:

$$c(\bar{\varepsilon}^{pl}) = c|_0 = c|_{\bar{\varepsilon}^{pl}=0} = 4 \text{ kPa}$$

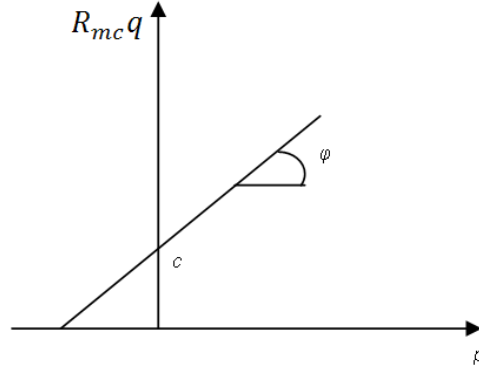


Figure 4.10: Mohr-Coulomb yield surface in the meridional plane. From ABAQUS 6.6 (2009).

Plastic flow

Flow of material at yield is governed by the plastic potential. The normality principle states that the plastic strain increment tensor is linearly related to the gradient of the plastic potential:

$$d\varepsilon^{pl} = d\lambda \frac{\partial G(\bar{\sigma})}{\partial \bar{\sigma}}$$

As proposed by Menétrey and William (1995), the flow potential is a hyperbolic function in the meridional stress plane and a smooth elliptic function in the deviatoric stress plane, defined as $\sigma_1 + \sigma_2 + \sigma_3 = 0$ (see Figure 4.11):

$$G = \sqrt{(\varepsilon c_{|0} \tan \psi)^2 + (R_{mw} q)^2} - p \tan \psi$$

where,

ψ is the dilation angle measured in the $p - R_{mw} q$ plane at high confining pressures. Clay is assumed to display no dilation, that is $\psi = 0^\circ$,

ε is the flow potential eccentricity in the meridional plane. The default value is used ($\varepsilon = 0.1$),

$c_{|0}$ is the initial cohesion yield stress (when there is no plastic strain), and

R_{mw} is the deviatoric elliptic function.

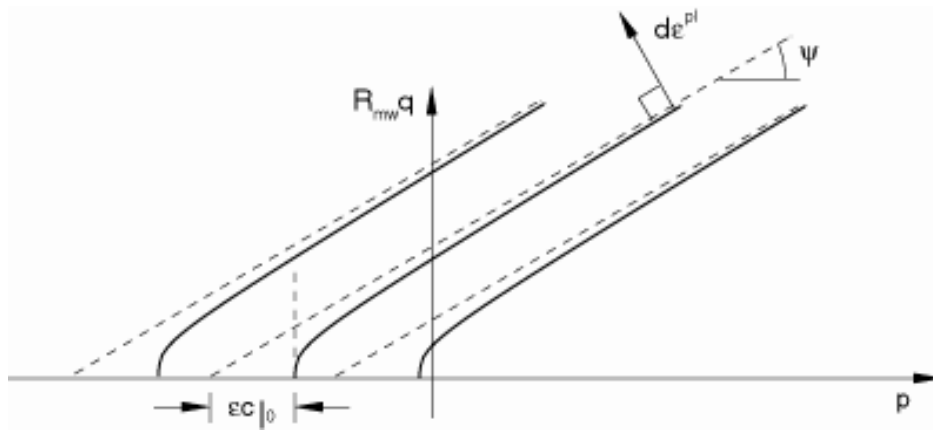


Figure 4.11: Family of hyperbolic flow potentials in the meridional stress plane. From ABAQUS 6.6 (2009).

Flow in the meridional stress plane is associated if the angle of friction and the angle of dilation are equal.

For practical reasons drainage is not simulated and pore water is not considered. Yet, considering friction without any pore pressure would overestimate the shear strength. That is why the undrained shear strength is used. Moreover, the experimental tests were assessed to be close to undrained, that is, the tests were performed relatively fast and almost no volumetric changes occurred. A more detailed explanation on drained and undrained shear strength can be found in Helwany (2007), see also Figure 4.12. The cohesion and the friction angle used for the clay are:

$$c_{u,clay} = 4 \text{ kPa}$$

$$\varphi = 0^\circ$$

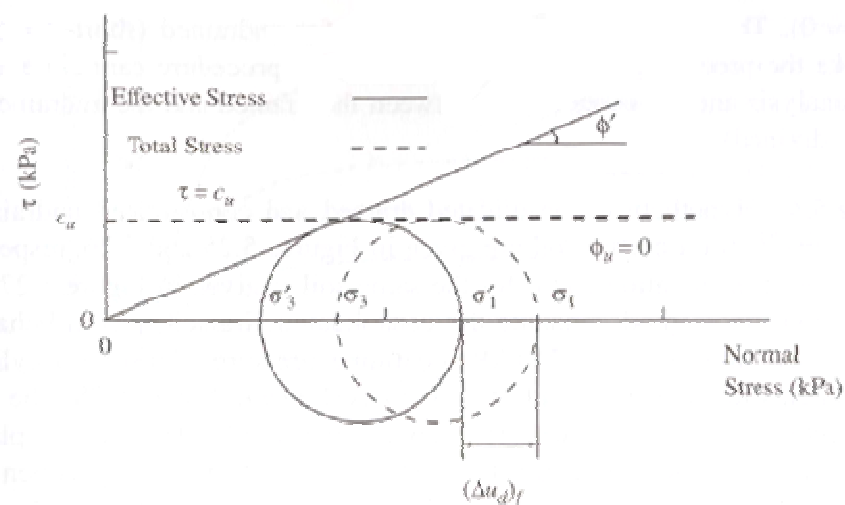


Figure 4.12: Drained and undrained strength parameters. From Helwany (2007).

4.2.4 Sand

The 50 mm sand layer was modeled as a linear elastic material. Its properties are gathered in Table 4.7.

Table 4.7: Basic mechanical properties of the sand.

Property	Value
Density [kg/m ³]	1800
Elastic modulus [MPa]	100
Poisson's ratio	0.3

4.3 Numerical analyses

4.3.1 Non-linear analyses

The complete load history of a simulation has to be divided into a number of steps. The type of response, or analysis procedure, can be different from step to step, for example static or dynamic response, frequency analysis. It is generally more computationally efficient to create separate steps for each part of the analysis, because contact analyses are much more difficult to complete if all the loads are applied in one step. Each step is a period of “time”. For each step ABAQUS calculates the response of the model to a particular set of loads and boundary conditions (the starting point for each step is thus the deformed state at the end of the previous step). The analysis procedures have here been carried out with a static general analysis procedure.

There are three sources of non-linearity in structural mechanics simulations – material, boundary and geometric non-linearity. In the present case, non-linearities arise from yielding and plastic behavior of the soil and columns caused by large deformations. ABAQUS can take into account non-linear effects of large displacements, deformations and other non-linear geometric effects through the option NLGEOM; if this setting is not included ABAQUS performs a geometrically linear analysis.

The objective of an analysis is to determine the load-displacement curve. Once the nodal displacements are known, the stresses and strains in each finite element can be determined easily. As the relationship between the force and the displacement is no longer linear, the structure's stiffness is dependent on the displacement. The solution is found by specifying the loading as a function of time and incrementing time to obtain the response. Each step of the simulation is therefore broken into increments. ABAQUS calculates the response to a small load increment using Newton's method, i.e. the displacement is calculated from the tangent stiffness K_0 (see Figure 4.13). If the force residual R_a , which is the difference between the total load applied and the internal forces, is less than a tolerance value, the structure is in approximate equilibrium (the solution is said to have converged) and the next increment starts. Unlike linear problems, the force residual will never be exactly zero in a non-linear analysis. Another iteration is performed if the force residual is too high.

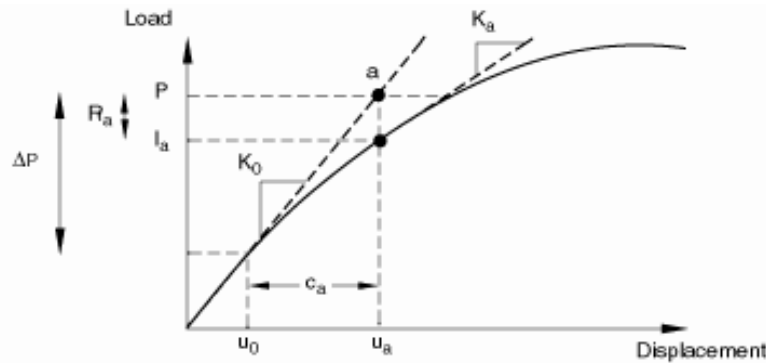


Figure 4.13: First iteration in an increment. From ABAQUS 6.6 (2009).

For each iteration in a non-linear analysis ABAQUS has to form and invert the structure's stiffness matrix, which makes it computationally much more expensive than a linear analysis. The computational cost of each iteration is close to the cost of conducting a complete linear analysis. Furthermore, the amount of data generated can be extremely high. Only the size of the first increment has to be specified. The size of the other increments can be automatically adjusted by ABAQUS, depending on the degree of non-linearity. Basically, if the solution converges too slowly, the size of the next increments is reduced. On the other hand, if the convergence of an increment is achieved fairly easily, the size is increased. The simulation stops if too many attempts were carried out for an increment (this is called the maximum number of cutbacks) or if the time increment required is smaller than the minimum specified. In the concrete damaged plasticity model the plastic potential is different from the yield function, which means that the plastic flow is non-associated. It requires therefore the solution of non-symmetric equations, i.e. non-symmetric stiffness matrix. To obtain an acceptable rate of convergence in ABAQUS/Standard, the unsymmetric matrix storage and solution scheme should be used.

In order to overcome convergence problems, default values of several parameters can be changed. For instance the maximum number of cutbacks allowed for an increment and the number of equilibrium iterations after which the check is made whether the residuals are increasing in two consecutive iterations can be increased. The force residual can be decreased.

4.3.2 Contact properties

The first step in defining contact between two structures in ABAQUS is to create contact surfaces. Next, pairs of surfaces that may contact each other are connected. When defining contact pairs the master surface and the slave surface must be précised. The distinction between those is important to achieve the best possible contact simulation as they are not equivalent. Nodes from the slave surface cannot penetrate the segments that make-up the master surface, but the master surface can penetrate the slave surface between slave nodes. The slave surface should be the more finely meshed surface. The difference is illustrated in Figure 4.14.

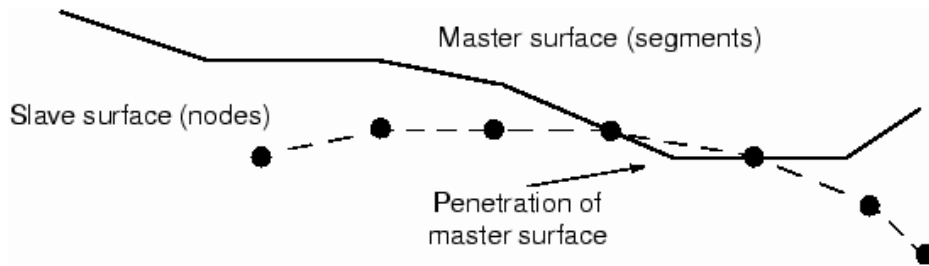


Figure 4.14: Difference between the master and the slave surfaces. From ABAQUS 6.6 (2009).

Tie constraint

A simple way to define contact is to use a tie constraint. It constraints two separate surfaces together so that there is no relative motion between them. Slave nodes are constrained to follow the motion of the closest master node. Nodes on the slave surface that are not within the tolerance distance are not tied. The default position tolerance is 5% of the typical element size in the master surface. This can alternatively be specified by the user. The tie constraints used in the model are detailed in section 4.3.4.

Normal and tangential behavior

In the most general contact cases between two bodies, a force normal to the contacting surfaces acts, as well as a tangential force if there is friction. Mechanical contact properties consist of the normal and tangential behaviors and have to be defined in order to be used with contact pairs.

Normal behavior between interacting surfaces is specified as a contact pressure-overclosure relationship. The contact constraint is applied when the clearance, the distance separating two surfaces, is zero. Any contact pressure can then be transmitted between the surfaces. The surfaces separate if the contact pressure becomes zero, and the constraint is removed. In other words the surfaces transmit no contact pressure unless the nodes of the slave surface contact the master surface. This surface interaction behavior, referred to as “hard” contact, is the default pressure-overclosure relationship in ABAQUS (Figure 4.15).

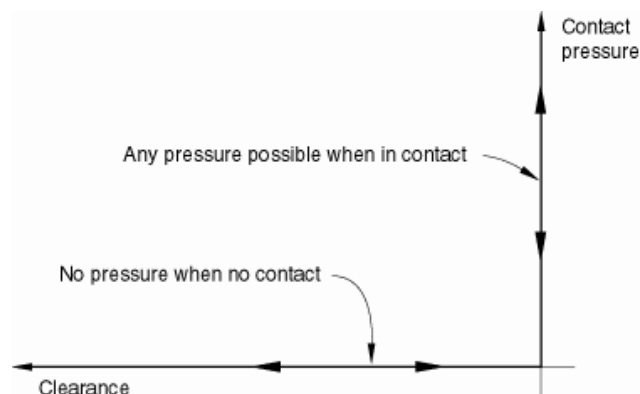


Figure 4.15: Default pressure-overclosure relationship. From ABAQUS 6.6 (2009).

The “hard” contact relationship can be modified to allow the surfaces to “overclose” by a certain distance before contact pressure is transmitted, and transmit “tensile” contact pressure. It is also possible to define “softened” contact relationships in which the contact pressure is a linear or exponential function of the clearance between the surfaces. Finally a no separation relationship can be used. It prevents surfaces from separating once they have come into contact.

Frictional behavior can be specified in terms of the classical isotropic Coulomb friction model. When defining contact pairs the magnitude of the relative sliding has to be chosen between small and finite. The basic concept of the Coulomb friction model is to relate the maximum allowable frictional (shear) stress across an interface to the contact pressure between the contacting bodies. In the basic form of the Coulomb friction model, two contacting surfaces can carry shear stresses up to a certain magnitude across their interface before they start sliding relative to one another; this state is known as sticking. The Coulomb friction model defines this critical shear stress, at which sliding of the surfaces starts as a fraction of the contact pressure, p , between the surfaces ($\tau_{crit} = \mu p$). The stick/slip calculations determine when a point transitions from sticking to slipping or from slipping to sticking. The fraction, μ , is known as the coefficient of friction (Figure 4.16). It can be defined in terms of slip rates, contact pressure and temperature. For the basic Coulomb friction model the only input data required is the coefficient of friction between the contacting surfaces. ABAQUS offers also the possibility to define a static and kinetic friction coefficient, i.e. friction between the surfaces is less after sliding has started, and a shear stress limit above which sliding will occur. Friction can also be specified as “rough” friction, the coefficient of friction is infinite and all relative sliding motion between two contacting surfaces is prevented. This model is often used with the no separation relationship.

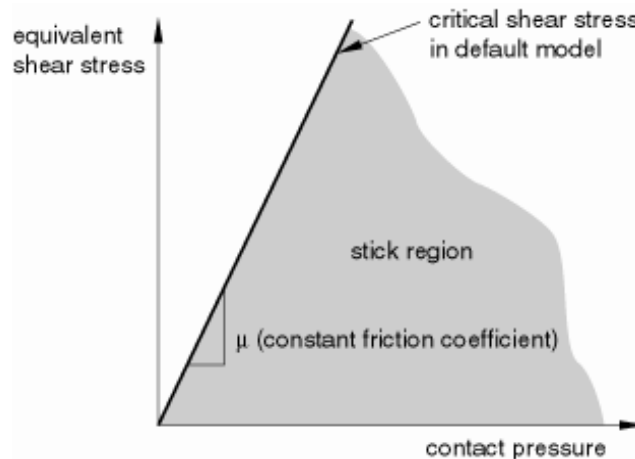


Figure 4.16: *Slip regions for the basic Coulomb friction model. From ABAQUS 6.6 (2009).*

The most realistic modeling of the interaction between the soil and the lateral sides of the columns is a combination of normal and tangential behaviors, that is, “hard” contact and Coulomb friction. It has been used for the FE analyses (see section 4.3.4).

4.3.3 Finite elements

The geometry of the model makes it impossible to mesh with brick elements. Tetrahedral elements are used instead. Second-order tetrahedral elements (C3D10) cannot be used here because they require too much computer power. Instead first-order tetrahedral elements (C3D4) are used (see Figure 4.17). This element has four nodes and one integration point. It provides accurate results only in general cases with very fine meshing (the element is too stiff) and it exhibits slow convergence with mesh refinement. However the analyses proved the C3D4 to be efficient. The typical number of elements was 100,000 for the soil and 20,000 per column.

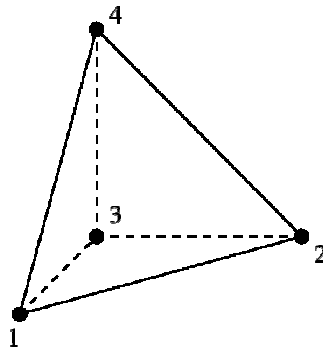


Figure 4.17: 4-node tetrahedral element (C3D4). From Dhont (2007).

4.3.4 Procedure

The procedure for numerical simulations on reinforced and unreinforced soils is similar; the only difference is the presence of columns. The geometry of the model is quite simple. It includes four parts:

- The soil,
- The sand layer,
- The columns (only for the analyses on reinforced soil), and
- A rigid plate. The plate reproduces the steel plate upon which the dead weight is applied.

The steel container is not modeled in order to save computer power and because the primary concern is the lime/cement columns. Instead, boundary conditions are used. The lower part of the cylinder is built-in during the whole analyses, as all six degrees of freedom are constrained. The FE model can be seen in Figure 4.18.

The simulation is basically run in two steps:

- Step 1: Gravity and the vertical load are applied in order to establish the initial state of stress within the materials. The vertical load consists in a force applied to the reference point (called master node) of the rigid plate. Its value corresponds to the pressure applied in the experimental tests, 10 kPa/1964 N for unreinforced soil and 15 kPa/2945 N for reinforced soil. All the nodes follow this

master node. During this step all translational degrees of freedom on the upper part (i.e. the outer surface of the clay and the sand) of the shear box are restrained ($U_1=U_2=0$). This reproduces fairly enough the steel container (assumed to be very stiff).

- Step 2: Gravity and the vertical load remain. The upper part of the shear box is now horizontally displaced. As the steel container is assumed to be very stiff, all the nodes on the upper surface are pulled in the second direction.

Several interactions are modeled as tie constraints, see Table 4.8. The contact definition between the lateral sides of the columns and the clay is described in section 4.2. Parts of the model had to be partitioned in order to avoid overconstraints, that is, a slave node having two masters.

Table 4.8: List of tie constraints.

Tie constraint	Master	Slave
1	Rigid plate	Sand
2	Sand	Upper surface of the clay and the columns
3	Clay	Lower surface of the columns

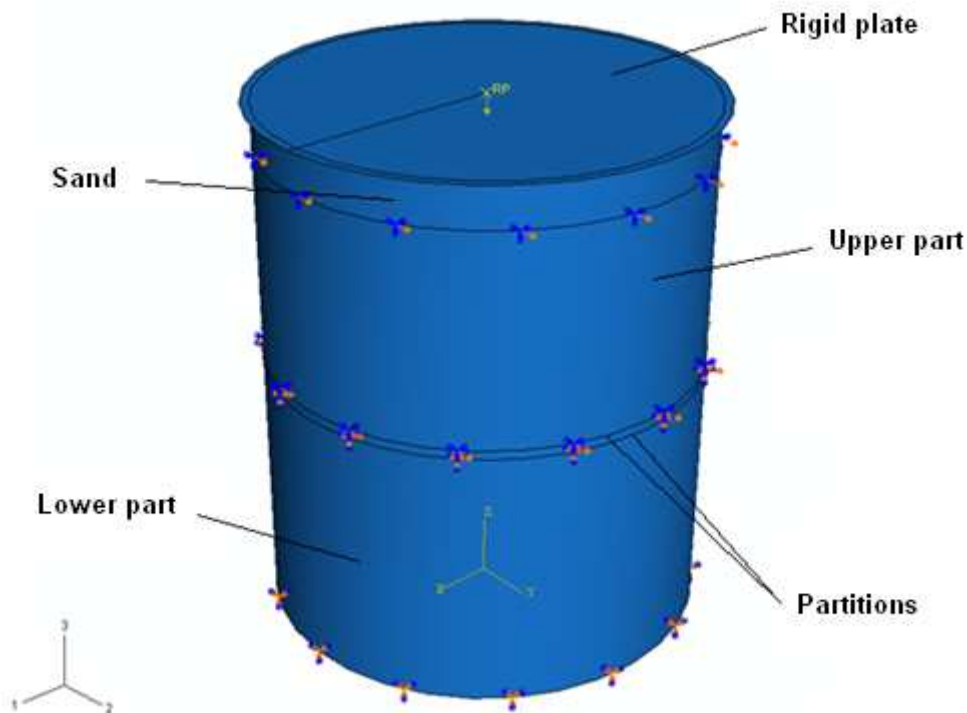


Figure 4.18: FE model.

The labeling convention used for the displacement and rotational degrees of freedom in ABAQUS is shown in Figure 4.19.

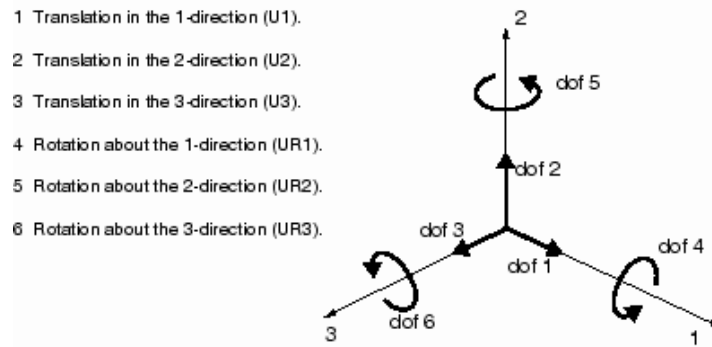


Figure 4.19: Displacement and rotational degrees of freedom.
 From ABAQUS 6.6 (2009).

FE analyses of unreinforced soil

The application of the shearing displacement is divided in 30 sub-steps in order to capture accurately enough the load-displacement curves and compare them to the experimental results. This increases the calculation time and the amount of data created. Each step is given the same duration (1). The first step – application of the vertical load and the gravity load – has also the duration 1. The displacement is applied as a linear function of time. Reaction forces in the second direction (RF2) from each upper node are then summed and the load-displacement curves can be plotted.

Convergence problems can occur due to the distortion of the clay elements when the displacements become too large. To overcome this, the soil was partitioned in the middle, using the *partition cell* option. New faces are created, which results in a “layer” of smaller elements that enforces the plasticizing of the clay around this location. The importance of this feature is further discussed in chapter 5. The mesh is showed in Figure 4.20.

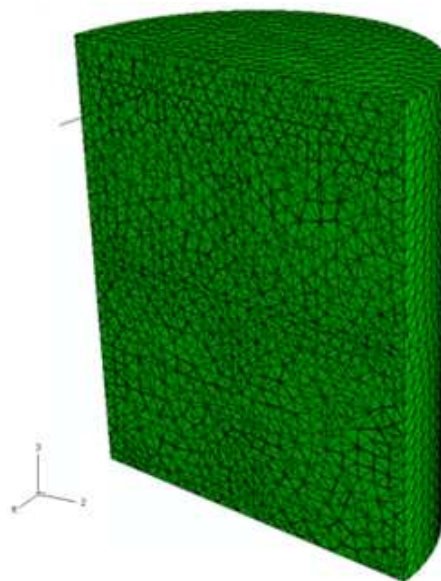


Figure 4.20: Mesh of the unstabilized soil.

FE analyses of reinforced soil

The FE model with 12 single columns is showed in Figure 4.21. The interaction between the lateral sides of the columns and the surrounding soil has been modeled with Coulomb friction for the tangential behavior and “hard” contact for the normal behavior, see section 4.3.2. The coefficient of friction was chosen small and varied from $\mu=0$ (i.e. frictionless behavior) to $\mu=0.1$. The meshing is the same as for the unstabilized soil, including the cell partition in the middle. The columns are meshed in a finer way than the soil, see Figure 4.21.

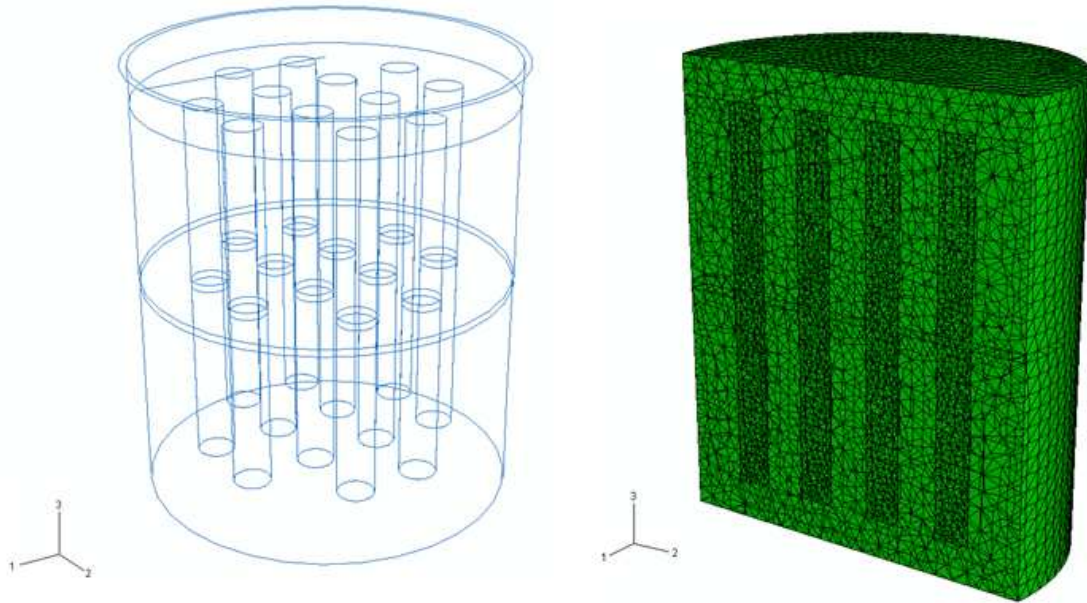


Figure 4.21: FE model and mesh with 12 single columns.

5 Results and discussion

5.1 Finite Element analyses of unstabilized soil

Numerical analyses on unstabilized soil were performed in order to adjust the linear elastic properties of the clay, that is, Young's modulus and Poisson's ratio. The deformed model and the horizontal displacement field (U2) are shown in Figure 5.1. Plasticizing in the "middle layer" can be clearly seen.

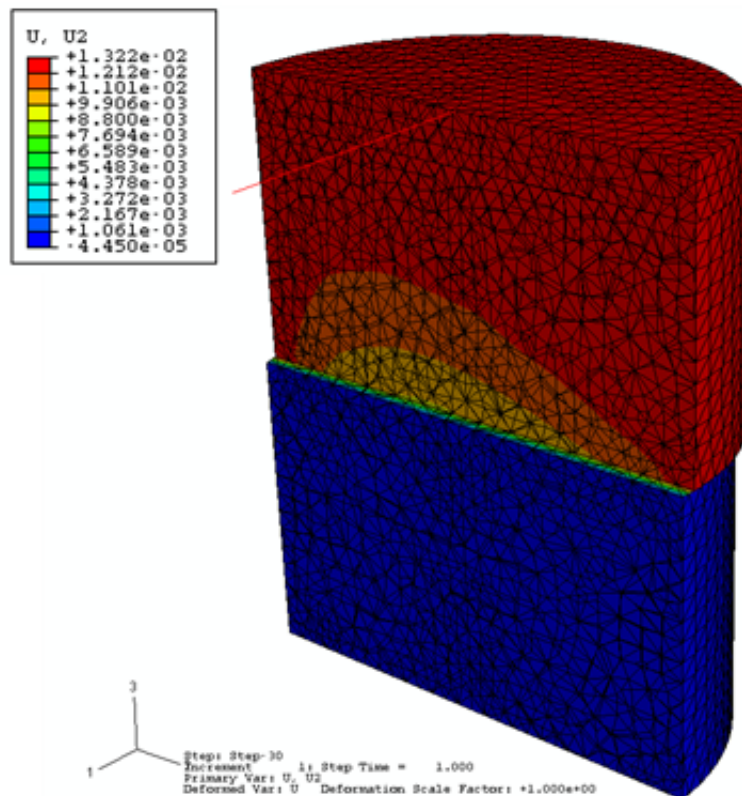


Figure 5.1: Horizontal displacement field of the unstabilized soil after shearing.

Several of the previous FE analyses (e.g. Kitazume and Maruyama, 2006) used 0.45 for Poisson's ratio. This high value is related to the almost-incompressible behavior of the clay – as the experiments were almost undrained, almost no water left the soil and almost no decrease of the volume occurred. It should be noted that the physical upper limit of Poisson's ratio, i.e. respecting thermodynamical laws, is 0.5. Several values of Young's modulus, ranging from 0.5 MPa to 4.5 MPa, have been

tested. The results are showed through load-displacement curves in Figure 5.2. The same procedure was repeated for Poisson's ratio equal to 0.48 and the results are showed in Figure 5.3. The influence of Poisson's ratio has also been studied and is showed in Figure 5.4. It was varied from 0.40 to 0.49, Young's modulus being kept constant at 2 MPa.

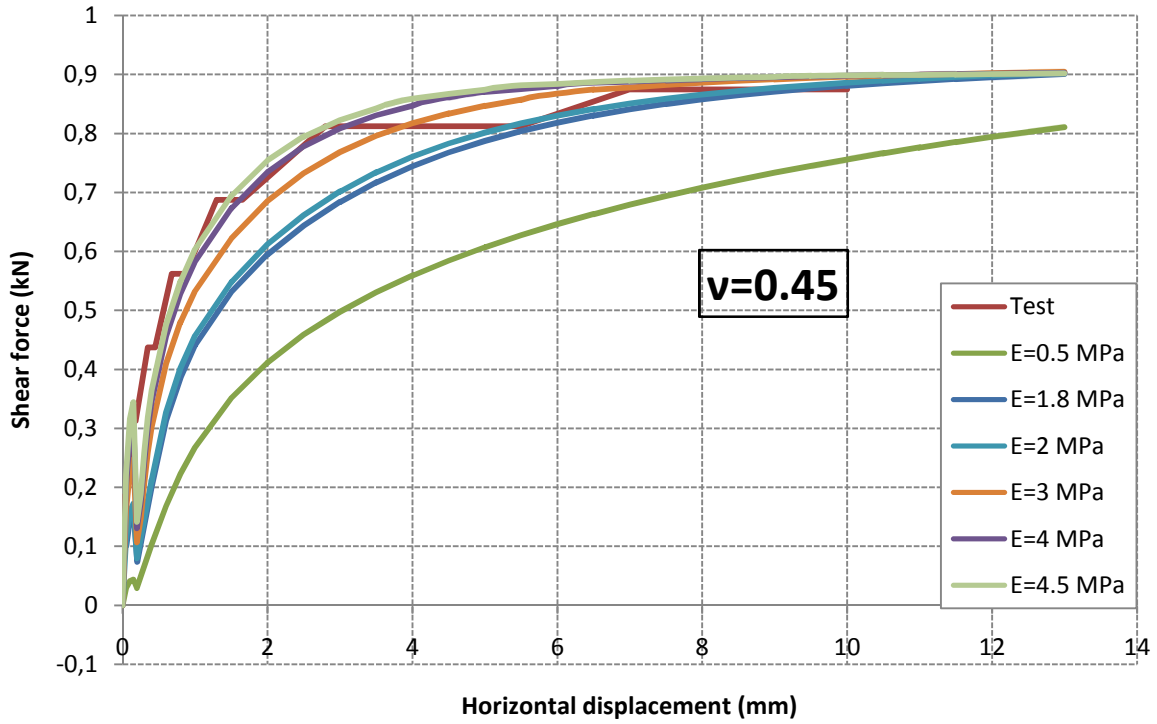


Figure 5.2: Experimental and numerical load-displacement curves.

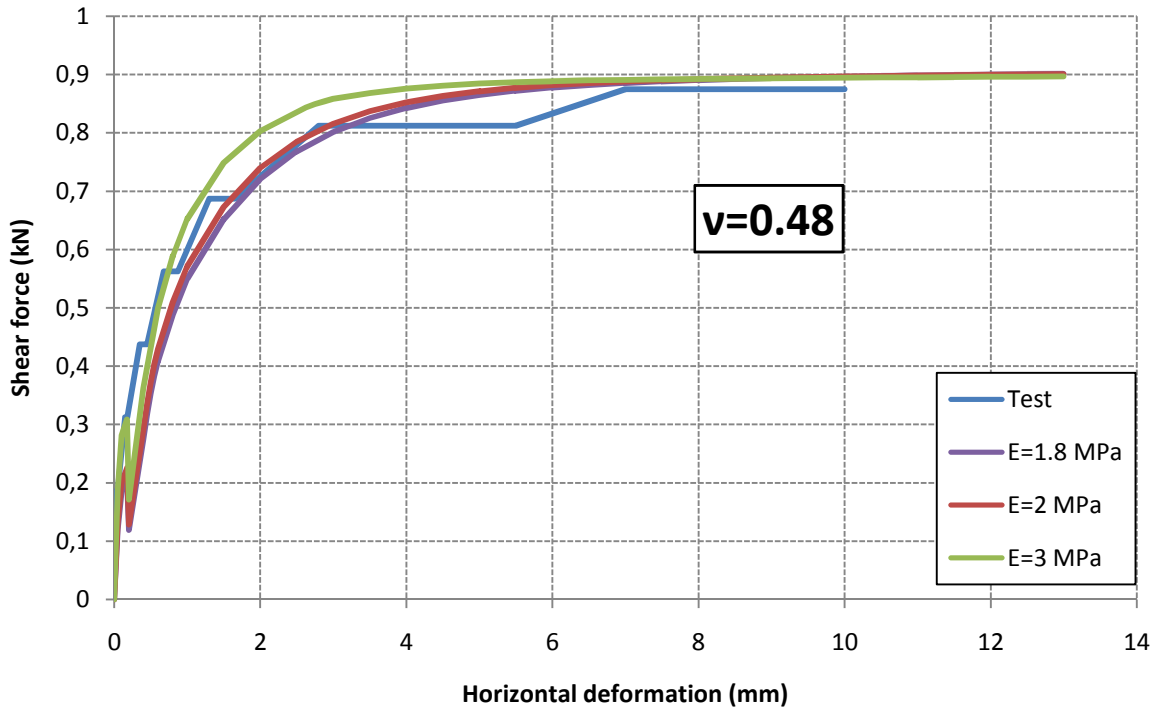


Figure 5.3: Influence of Young's modulus.

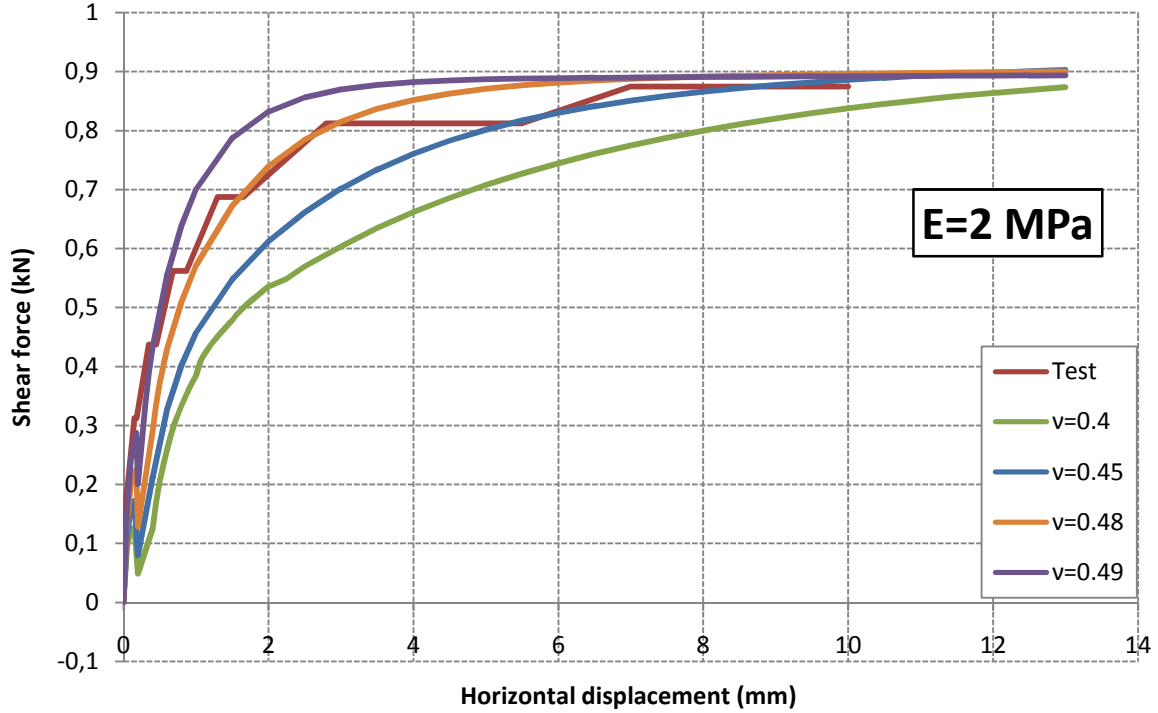


Figure 5.4: Influence of Poisson's ratio.

It can be seen from the load-displacement curves that several combinations of Young's modulus and Poisson's ratio could fit the experimental results. Using $E=4$ MPa probably overestimates the actual stiffness. Indeed the clay is modeled as an elastic-perfectly plastic material, underestimating thus the initial stiffness. Moreover, the Mohr-Coulomb model does not account for stiffness degradation when large deformations occur, whereas it is the case for the concrete damaged plasticity model used for the lime/cement columns. This implies that, under large deformations, the column might be weaker than the surrounding soil, which is rather unrealistic. Another limiting effect is the fact that Young's modulus of the clay is actually lower after some deformations have occurred. This is not too much of a problem for the tests on unstabilized soil, but it has to be considered when lime/cement columns are present. Using a "larger" Young's modulus for the clay (a typical value is 2 MPa) is realistic at the beginning of the shearing but is not relevant afterwards – the ultimate load would then be too high. Since we are interested in the failure of the reinforced soil, lower values of Young's modulus of the clay will be used, between 0.5 MPa and 1 MPa. Poisson's ratio is taken as ranging from 0.45 to 0.48.

Brief mesh and step refinement analyses were also performed with $E=4$ MPa being used, but the results would not be different with another modulus. The seed is the average size of the clay elements (the values are given in m). Neither decreasing the size of the elements nor applying the load in more steps, in order to capture the trend more precisely, changes the results as seen in Figures 5.5 and 5.6.

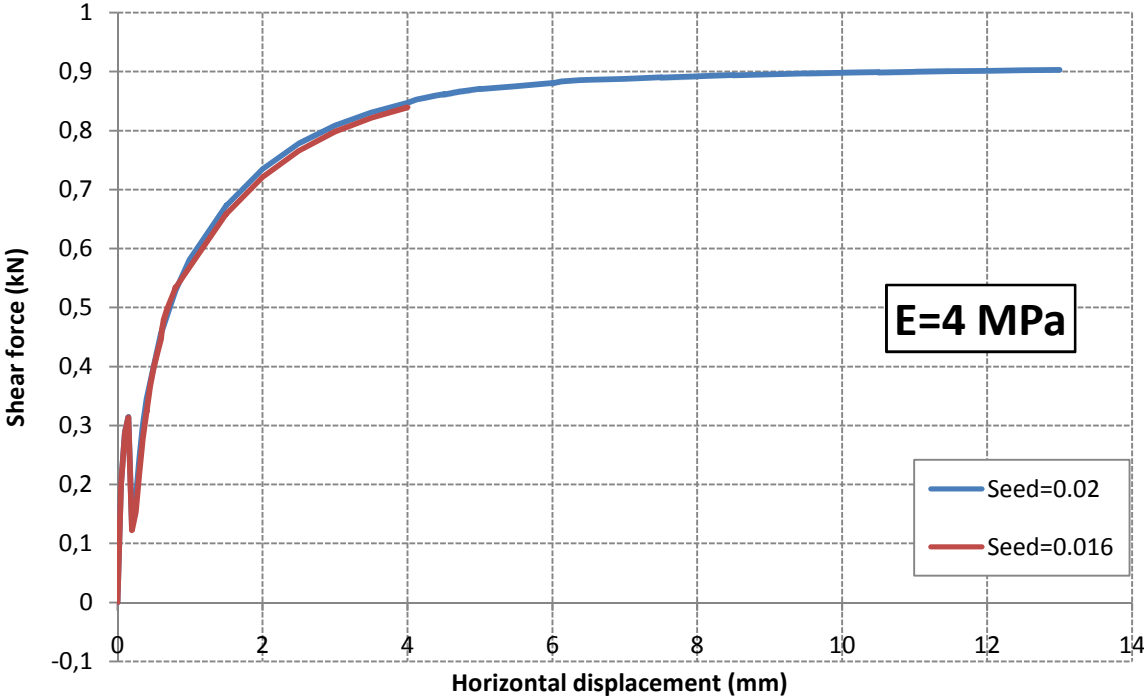


Figure 5.5: Influence of the mesh density.

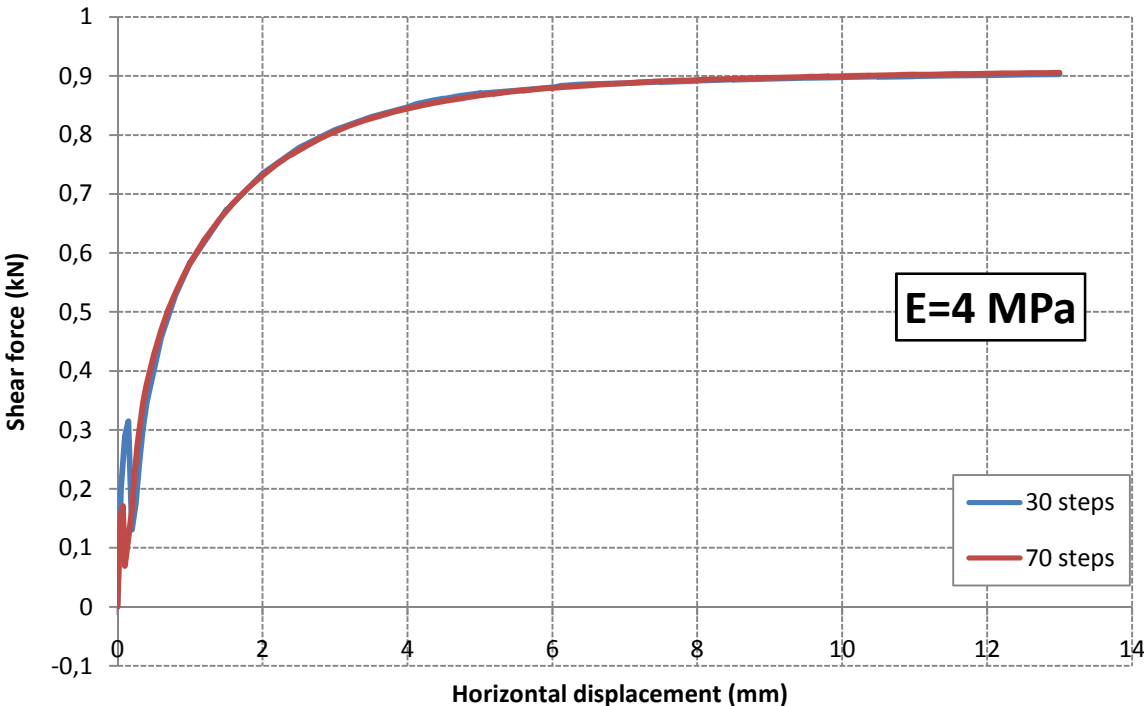


Figure 5.6: Influence of the number of steps.

5.2 Finite Element analyses of stabilized soil

Failure of lime/cement columns is the main concern of this thesis. FE analyses have been performed with 12 single columns. The concrete damaged plasticity model does not allow for a direct visualization of the cracks. They can however be observed through the damage tensile parameter d_t , which indicates a degradation of the material stiffness. A tensile crack is assumed to appear when the tensile strength of an element is lost i.e. when d_t has reached its maximum value, typically 0.9. It is also possible to visualize the crack width by multiplying the crack opening strain with the characteristic length of an element. A more detailed discussion on cracks visualization is given by Malm (2009). It is however reasonable to assume that cracks are formed, or are about to appear, even when d_t is less than its maximum value. This indicates isolated micro-cracks, which, upon larger deformations, will join and form one macro crack. Impurities within the columns (such as voids) lead furthermore to quicker cracking.

The horizontal displacement field after shearing is showed in Figure 5.7. A comparison with the case of unstabilized soil is showed in Figure 5.8, where the view cut is done in the middle of the model, which is the reason why the columns cannot be seen. Lime/cement columns clearly reduce the displacement of the soil between the columns.

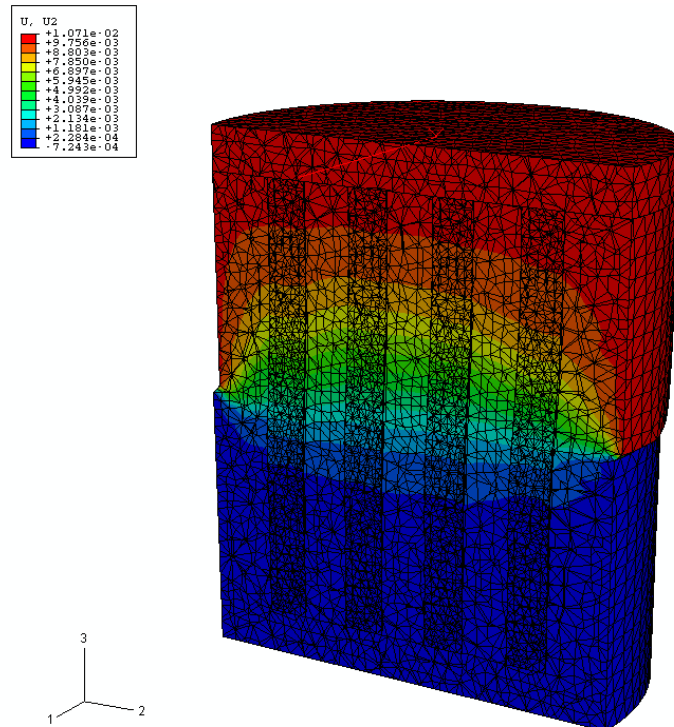


Figure 5.7: Horizontal displacement field of the stabilized soil after shearing.

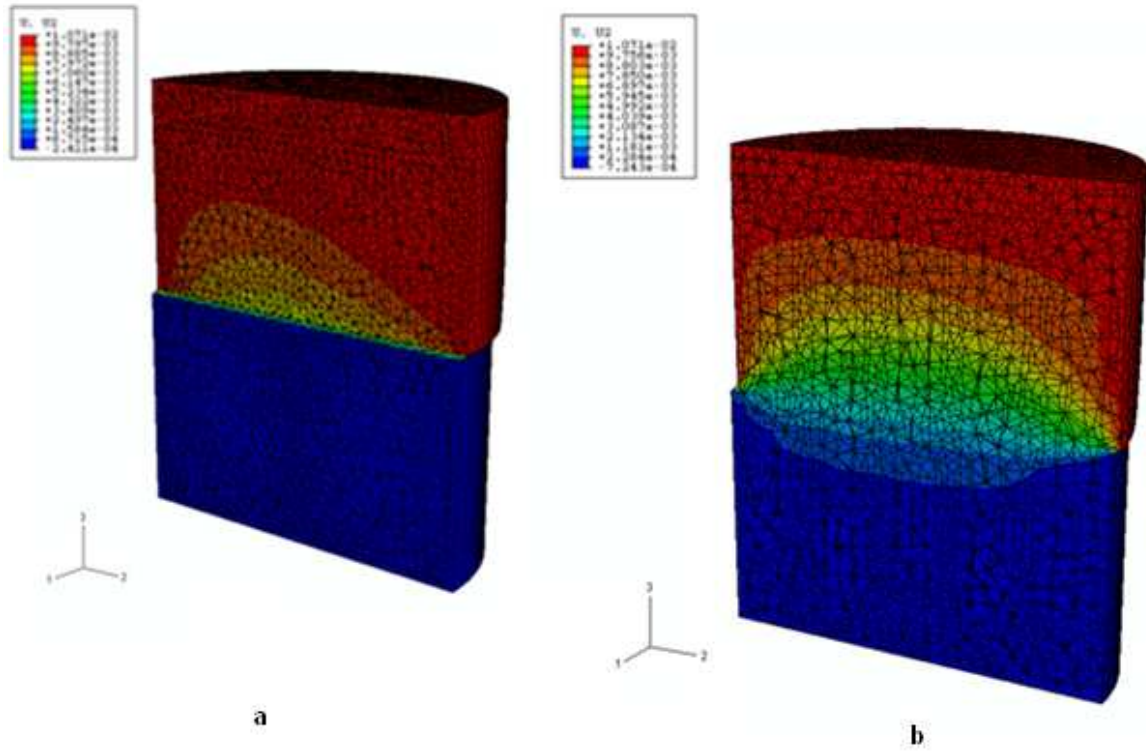


Figure 5.8: Horizontal displacement field of unstabilized and stabilized soil.

Figure 5.9 displays the deformed columns with the tensile damage parameter d_t . It is reasonable to assume that the zones where tensile damage occurs will lead to cracks. A range of four columns is also showed from the back and the front sides (Figure 5.10). The formation of plastic hinges is clearly visible.

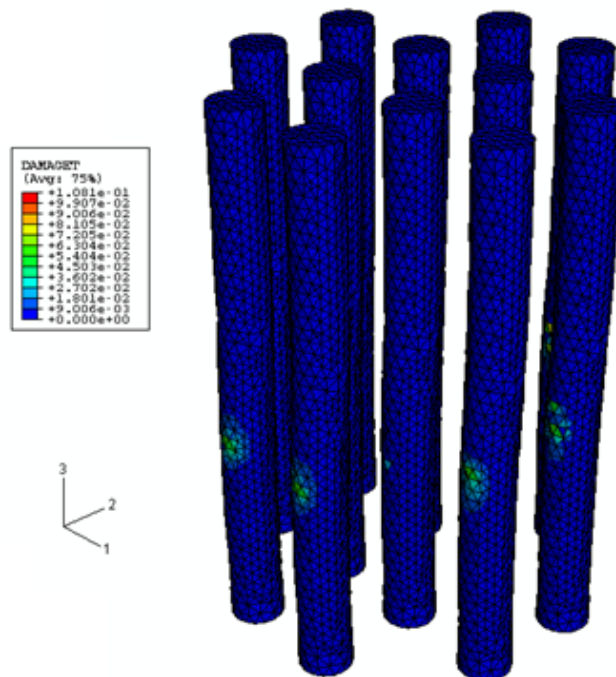


Figure 5.9: Formation of plastic hinges and tensile damage parameter.

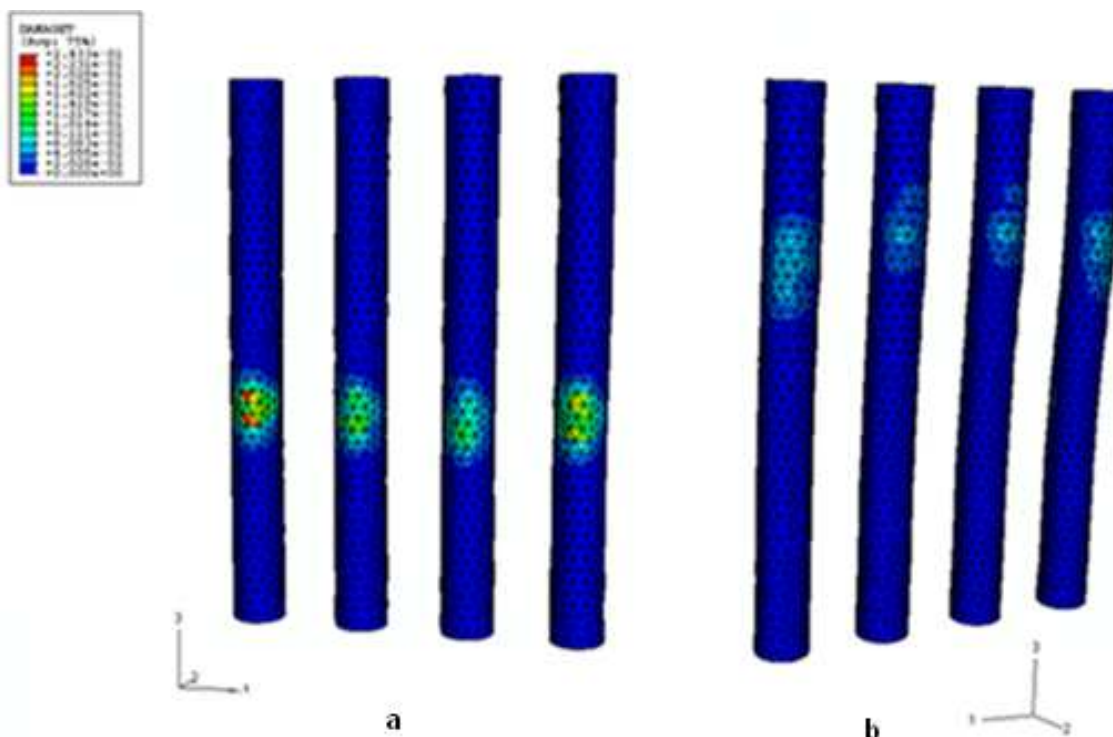


Figure 5.10: Deformed columns and tensile damage parameter (back and front).

The experimental and numerical load-displacement curves are showed in Figure 5.11 (with the vertical load). The results obtained from the FE analyses are in fairly good agreement with the experimental results. The ultimate load is about the same value – between 1 and 1.2 kN. The curves obtained from numerical analyses are less stiff in the beginning; this is because the elasticity of the clay is in reality lower when deformations are large. Hence a lower value has to be chosen in order to obtain a reasonable ultimate load (see section 5.1). Convergence problems occur when the shearing displacement reaches 7 - 8 mm. This is thought to be due to yielding of the materials, especially cracking and stiffness degradation of the lime/cement columns. Both cases with and without a vertical loading are displayed in Figure 5.12. The vertical confinement increases the ultimate load, but this effect is minor. For purely practical reasons, the material parameters are slightly different for Figures 5.11 and 5.12: in Figure 5.11 the cohesion of the clay is 3 kPa, Young's modulus of the clay is 1 MPa and the tensile strength of lime/cement is 8 kPa. In Figure 5.12 these parameters are 4 kPa, 0.8 MPa and 10 kPa respectively. Using the same material properties would give similar results.

The FE analyses on single columns confirmed the experimental results from Larsson (2008) and the conclusions from Kivelö (1998), Adams et al. (2009) and Kitazume et al. (2009): the columns fail by bending, that is, plastic hinges are formed where the moment capacity is exceeded, see Figure 5.13. The distance between the plastic hinges is found to be approximately the same as in the experimental tests, about 10 cm. The FE analyses have also showed that the columns fail one by one in the bending failure mode in sequence from the forefront to the rearmost column, as previously pointed out by Kitazume et al. (2009). Because they solely consider shear failure, which is less probable than bending failure, the current design methods might in some cases overestimate the stability of the embankments.

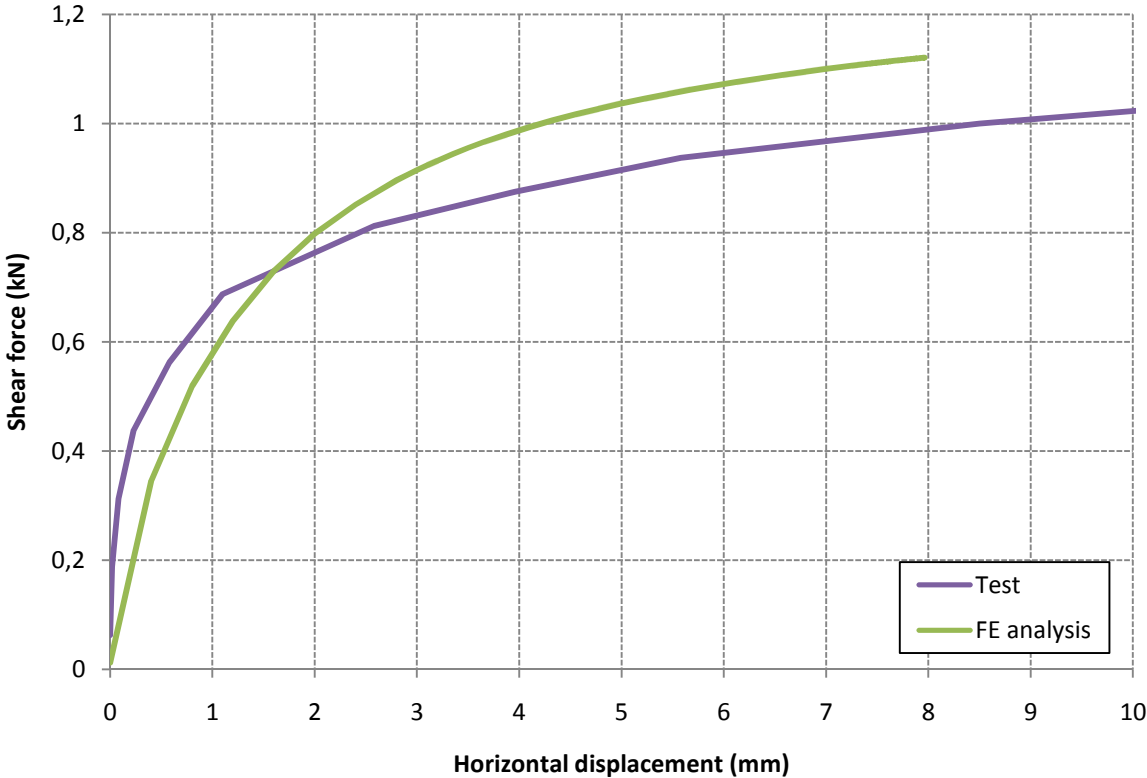


Figure 5.11: Experimental and numerical load-displacement curves.

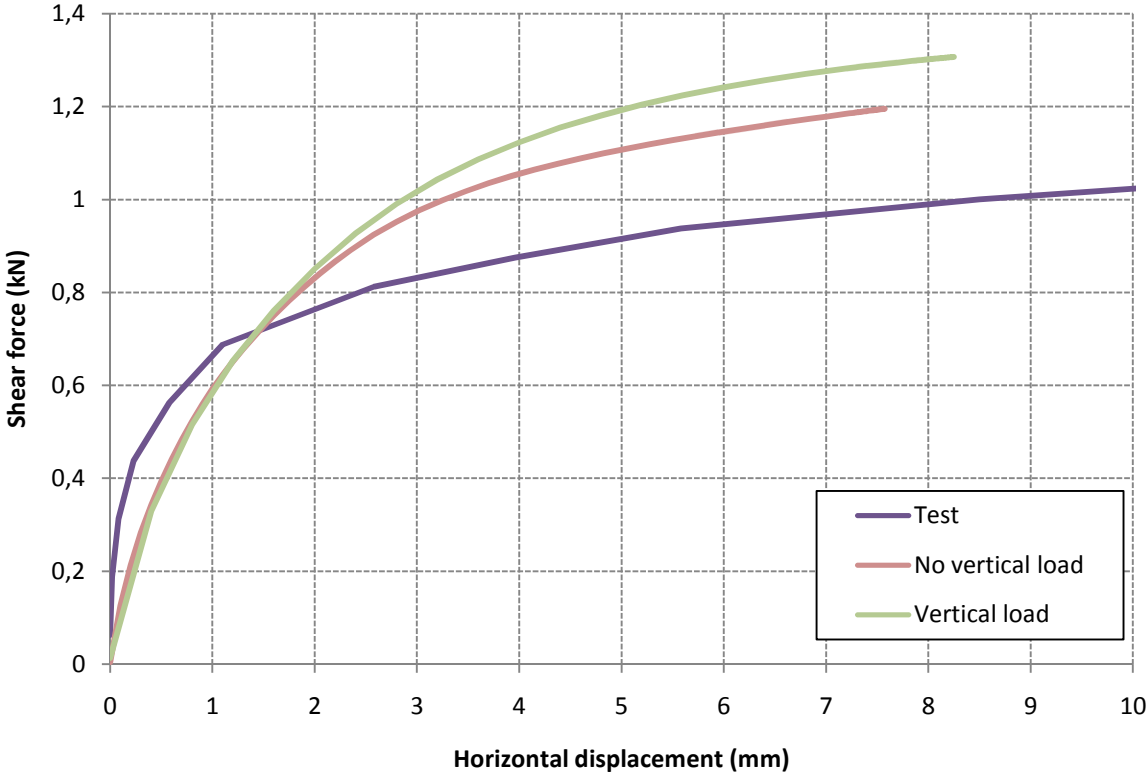


Figure 5.12: Influence of the vertical load.

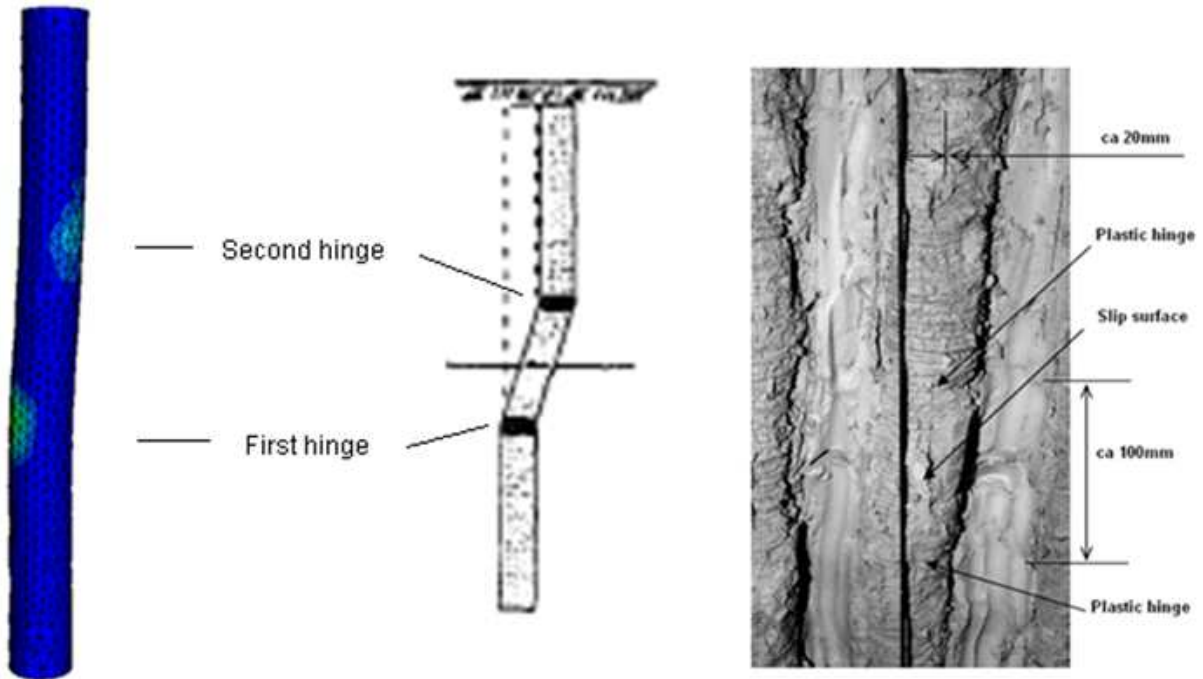


Figure 5.13: Location of the plastic hinges. Results from ABAQUS, Kivelö (1998) and Larsson (2008).

Kivelö (1998) proposed a formula to estimate the dowel force at the slip surface, see Figure 5.14:

$$T_{col} = kc_u df$$

where,

k is the bearing capacity factor,

c_u is the undrained shear strength of the unstabilized soil,

d is the column diameter, and

f is the distance between the failure surface and the plastic hinge.

The observations on the columns give $f = 50$ mm. According to Broms (1999), a low value of the bearing capacity factor, $k = 2$, can be used for low strength columns, that is, when the shear strength of the soft soil divided by the unconfined compression strength of the column material is greater than 0.04. This ratio is here equal to $\frac{4.4}{60} = 0.073$. This yields a dowel force equal to 22 N, hence 264 N for 12 single columns. The shear resistance of the unstabilized soil is estimated as $T_{soil} = A_{soil}c_u$, where A_{soil} is the area of the clay (88 % of the total area). Then $T_{soil} = 777$ N. The shear resistance of the stabilized soil is then:

$$T_{total} = T_{soil} + T_{col} = 1.041 \text{ kN}$$

i.e.

$$\tau = \frac{T_{total}}{area} = 5.3 \text{ kPa}$$

This value is in fairly good agreement with the experimental and numerical values (see Figures 2.6 and 5.11).

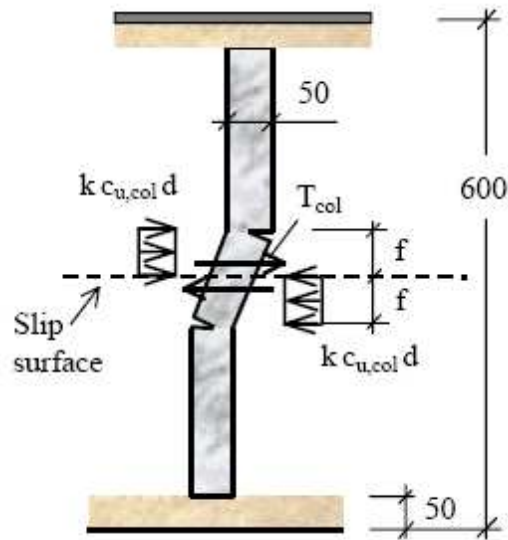


Figure 5.14: Failure mechanisms for the single columns. From Larsson and Broms (2000).

Convergence problems have been encountered when the deformations were important, because no clear failure of the soil could happen. This is the reason for partitioning the soil in the middle section, which enforces the plasticizing of the clay in the vicinity of this “layer”. This partition, obtained through the *partition cell* option, appears to be fundamental. In the case of unstabilized soil, complete shearing couldn't happen without this feature. In the case of stabilized soil with 12 single lime/cement columns, no clear failure happened, that is, the reinforced soil was too strong. This can be seen in Figure 5.15. It should be noted that without this partition, almost all changes in the material parameters, such as Young's modulus of the clay or the strength properties of lime/cement, or the friction coefficient, were effectless. Convergence problems have also been caused by the cracking of lime/cement columns, resulting in many very small increments (typical size of 10^{-6}). A way to overcome these problems – at least partially – is to change the tolerance values (see section 4.3.1).

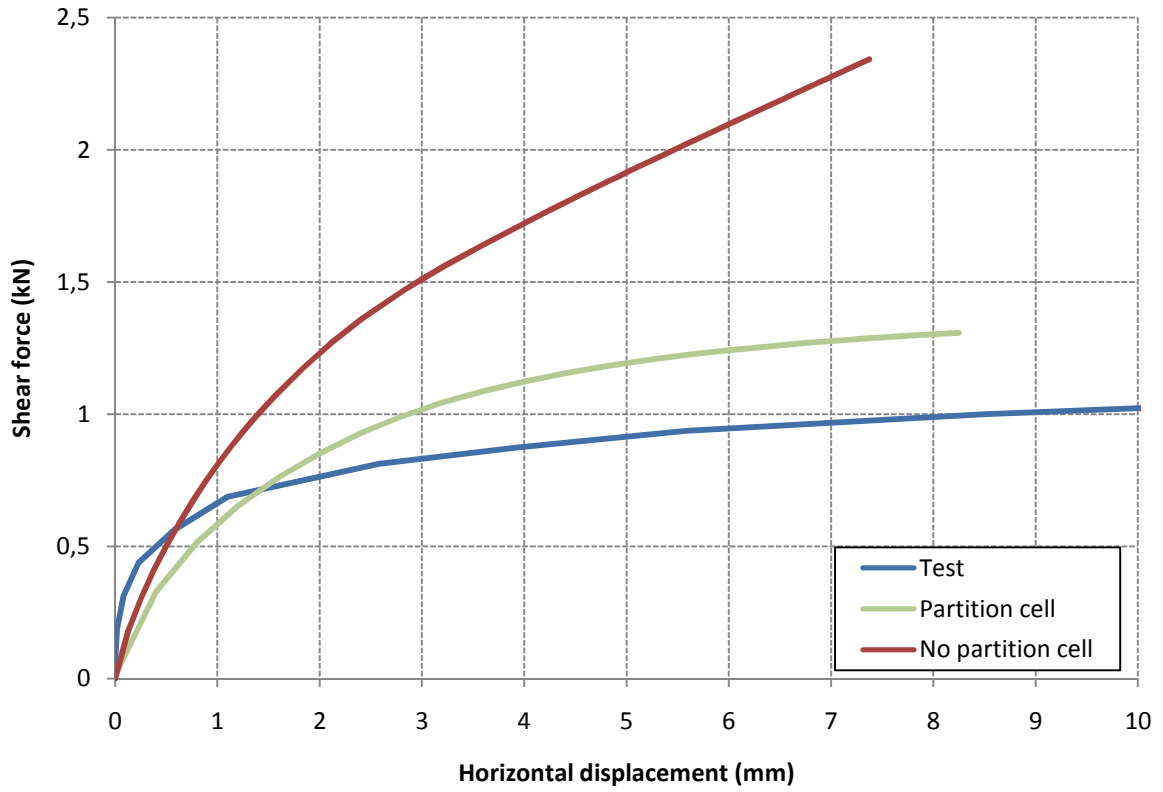


Figure 5.15: Importance of the cell partitioning.

6 Conclusions

6.1 General conclusions

The aim of this Master thesis was to numerically reproduce some of the experimental tests carried out by the Swedish Deep Stabilization Research Centre on lime/cement column stabilized kaolin clay. A recently developed material model – the concrete damaged plasticity model – was used for lime/cement for its ability to simulate cracks in order to capture more realistic failure modes. Numerical analyses were first carried out on unreinforced soil in order to calibrate the linear elastic properties. The results displayed fairly good agreement with the experimental tests. The second step – and the main interest of this work – was to simulate the behavior of lime/cement column reinforced soil under shearing. The simplest configuration – 12 single columns – was considered. It has been found that the concrete damaged plasticity model was suitable to simulate lime/cement columns, as the results were in good agreement with the experimental tests and previous theoretical and numerical analyses. The most important conclusion to be drawn is that the single columns fail by bending rather than shearing, which is in agreement with previous theoretical and experimental works. This is why the current design methods may overestimate the stability of the reinforced embankment, since they do not consider the most probable failure mode.

The principal limitations in the numerical analyses are due the large amount of parameters and variables, and the lack of knowledge regarding them. Young's modulus and Poisson's ratio of the materials were not well known, and several calibrations had to be performed. Undrained analyses were very sensitive to Poisson's ratio. Many of the input values required by the models for clay and lime/cement are not well known, and had to be tested to approach experimental results.

Among all the parameters required by the concrete damaged plasticity model, only the uniaxial compressive behavior data were actually obtained from uniaxial compressive tests on lime/cement columns. The scatter in the results was however quite large. Inhomogeneities within the materials can also explain the divergences from the experimental tests. The water content was significantly lower between the columns than in the outer part of the shear box. It was also low in the upper part, probably due to the sand layer.

For all the other parameters, either default values were used, or they were derived from concrete, for which the knowledge is much wider, considering the fact that lime/cement is a weaker and more brittle material. Such methods might be a cause for differences between the experimental results. For instance the ratios σ_{b0}/σ_{c0} and K_c describe biaxial and triaxial behaviors respectively. Since no experimental data are

available for lime/cement, concrete default values were used. This means that even with reliable uniaxial behavior data, the material under a general state of stress may be overestimated.

The concrete damaged plasticity model requires the following data:

- The dilation angle ψ ,
- The eccentricity ε ,
- The ratio σ_{b0}/σ_{c0} ,
- The ratio K_c ,
- The compressive yield stress σ_c as a tabular function of the inelastic strain $\tilde{\varepsilon}_c^{in}$,
- The tensile postfailure stress σ_t as a tabular function of the cracking displacement u_t^{ck} , and
- The tensile damage parameter d_t as a tabular function of the cracking displacement u_t^{ck} .

The Mohr-Coulomb plasticity model requires the following data:

- The meridional eccentricity ε ,
- The friction angle φ ,
- The dilation angle ψ , and
- The cohesion yield stress c as a tabular function of the plastic strain ε^{pl} .

The cohesion has been derived from the measurements on clay samples. The friction angle was taken equal to zero, because the undrained shear strength was used.

6.2 Suggestions for future research

Apart from more numerous and accurate experimental data regarding the properties of the materials (see section 6.1), other improvements can be done. Increasing computer power should make it possible to run finer and quicker analyses in a near future. Efforts should also be dedicated to solving convergence problems. Other major improvements concern the material modeling of the clay. It has been modeled using the elasto-plastic Mohr-Coulomb model with undrained shear strength. Simulating pore water would make it possible to use the drained shear strength and simulate the consolidation stage. The approximations used for the shear strength of the clay would no longer be necessary. Using a new plastic model such as Drucker-Prager or Cam clay is also expected to improve the accuracy of the results.

Bibliography

Adams, T., Filz, G.M., Navin, M.P., 2009. Stability of embankments and levees on deep-mixed foundations. *International Symposium on Deep Mixing and Admixture Stabilization*, Okinawa, 19-21 May. Paper DI-1.

Ansell, A., Malm, R., 2008. Modeling of thermally induced cracking of a concrete buttress dam. *Nordic Concrete Research*, Vol. 38, No. 2, pp. 69-88.

CDIT, 2002. *Deep Mixing Method – Principle, Design and Construction*. Edited by Coastal Development Institute of Technology (CDIT), Japan. Balkema Publishers, 123 pp..

Chen, W. F., Han D.J., 1988. *Plasticity for Structural Engineers*. Springer-Verlag, New York.

Filz, G.M., 2006. *Load transfer, settlement, and stability of embankments founded on columns installed by deep mixing methods*. Geotechnical Engineering Seminar Presentation, National Technical University of Athens.

Filz, G.M., Navin, M.P., 2006. *Stability of column-supported embankments*. Virginia Polytechnic Institute and State University.

Han, J., Parsons, R.L., & Huang, J., and Sheth, A.R. 2005. Factors of safety against deep-seated failure of embankments over deep mixed columns. *Proceedings of the International Conference on Deep Mixing, Best Practice and Recent Advances*, Stockholm, Vol. 1, pp. 231–236.

Helwany, S., 2007. *Applied Soil Mechanics with ABAQUS Applications*. John Wiley & Sons, Hoboken, NJ.

Hillerborg, A., M. Modeer, Petersson P.E., 1976. Analysis of Crack Formation and Crack Growth in Concrete by Means of Fracture Mechanics and Finite Elements. *Cement and Concrete Research*, Vol. 6, pp. 773–782.

Itasca Consulting Group, 2002. *FLAC2D Fast Lagrangian Analysis of Continua*. Itasca Consulting Group, Minneapolis, MN, USA.

Kitazume, M., Maruyama, K., 2006. External stability of group column type deep mixing improved ground under embankment loading. *Soils and Foundations*, Vol. 46, No. 3, pp. 323-340.

- Kitazume, M., Maruyama, K., Hashizume, H., 2009. Centrifuge model tests on failure modes of deep mixing columns. *Proceedings of the International Symposium on Deep Mixing and Admixture Stabilization*, Okinawa, 19-21 May. Paper DI-7.
- Kitazume, M., Hayano, K., Khan, M.R.A., 2008. Investigation on static stability of sheet pile quay wall improved by cement treated sea-side ground from centrifuge model tests. *Soils and Foundations*, Vol. 48, No. 4, pp. 563-575.
- Kivelö, M., 1998. *Stabilization of embankments on soft soil with lime/cement columns*. Doctoral thesis, Royal Institute of Technology, Stockholm.
- Kivelö, M., Broms, B.B., 1999. Mechanical behavior and shear resistance of lime/cement columns. *Proceedings of the International Conference on Dry Mix Methods: Dry Mix Methods for Deep Soil Stabilization*, pp. 193-200.
- Larsson, S., 1999. Shear box apparatus for modeling chemical stabilized soil – Introductory tests. *Proceedings of the International Conference on Dry Mix Methods for Deep Soil Stabilization*, Stockholm, 13-15 October, pp. 115-121.
- Larsson, S., 2005. State of Practice Report Session 6: Execution, monitoring and quality control. *Proceedings of the International Conference on Deep Mixing, Best Practice and Recent Advances*, Stockholm, vol. 2, pp. 732-785.
- Larsson, S., 2008. *Skjuvboxförsök på jordförstärkt kaolinlera med kalkcementpelare (shear box tests on lime-cement column improved kaolin)*. Arbetsrapport, Swedish Deep Stabilization Research Centre (in Swedish).
- Larsson, S., Broms, B.B., 2000. Shear box model tests with lime/cement columns – some observations of failure mechanisms. *Proceedings of the International Conference on Dry Mix Methods*, Melbourne, 19-24 November.
- Lee, J., Fenves, G.L., 1998. Plastic-damage model for cyclic loading of concrete structures. *Journal of Engineering Mechanics*, pp. 892-900.
- Lublinter, J., Oliver, J., Oller, S., Oñate, E., 1989. A plastic-damage model for concrete. *International Journal of Solids and Structures*, pp. 229-326.
- Malm, R., 2009. *Predicting shear type crack initiation and growth in concrete with non-linear finite element method*. Doctoral thesis, Royal Institute of Technology, Stockholm.
- McManus, K.J., Kulhawy, F.H., 1991. A cohesive soil for large-size laboratory deposits. *ASTM. Geotechnical Testing Journal*, Vol. 14, No. 1, pp. 26-34.
- McManus, K.J. and Kulhawy, F.H., 1993. Preparation of large-size laboratory deposits of cohesive soils. *ASTM. Geotechnical Testing Journal*, Vol. 16, No. 3, pp. 372-383.
- Menétrey, Ph., Willam, K.J., 1995. Triaxial failure criterion for concrete and its generalization. *ACI Structural Journal*, Vol. 92, pp. 311–318.
- Porbaha, A., 1998. State of the art in deep mixing technology: part I. Basic concepts and overview. *Ground Improvement*, Vol. 2, pp. 81–92.

SGF (2000). Lime and lime cement columns. Guide for design, construction and control. Report 2:2000, Swedish Geotechnical Society, Linköping, 111 pp. (in Swedish).

Terashi, M., 2003. The state of practice in deep mixing methods. *ASCE, Geotechnical Special Publication No. 120*, Vol. 1, pp. 25–49.

Vägverket, 2009. *Tekniska kravdokument Geo. VV Publ 2009:46.* Vägverket, Borlänge, (in Swedish).

Wright, S.G., 1999. *UTEXAS4: A Computer Program for Slope Stability Calculations.* Shinoak Software, Austin, TX, USA.

Internet pages

ABAQUS 6.6., 2009. Online manual, SIMULIA, Providence, RI, USA.

ABAQUS/CAE, 2009. http://www.simulia.com/products/abaqus_cae.html. SIMULIA, Providence, RI, USA.

ABAQUS/Standard, 2009. http://www.simulia.com/products/abaqus_standard.html. SIMULIA, Providence, RI, USA.

ABAQUS/Explicit, 2009. http://www.simulia.com/products/abaqus_explicit.html. SIMULIA, Providence, RI, USA.

Dhont, G., 2007. *CalculiX CrunchiX USER'S MANUAL 1.6.* http://web.mit.edu/calculix_v1.6/CalculiX/ccx_1.6/doc/ccx/ccx.html

Plaxis 2D, 2008. <http://www.plaxis.nl>. PLAXIS BV, Delft, The Netherlands.